AWARD NUMBER: W81XWH-16-1-0562

TITLE: Targeting the HSP40/HSP70 Molecular Chaperone Axis as a Novel Treatment Strategy for Castrate-Resistant Prostate Cancer

PRINCIPAL INVESTIGATOR: Dr. Leonard Neckers

CONTRACTING ORGANIZATION: Geneva Foundation, Tacoma, WA

REPORT DATE: October 2022

TYPE OF REPORT: Annual

PREPARED FOR: U.S. Army Medical Research and Development Command
Fort Detrick, Maryland 21702-5012

REPORT DOCUMENTATION PAGE

Form Approved OMB No. 0704-0188

1. REPORT DATE	2. REPORT TYPE	3. DATES COVERED
October 2022	Annual	30Sep2021-29Sep2022

4. TITLE AND SUBTITLE

Targeting the HSP40/HSP70 Molecular Chaperone Axis as a Novel Treatment Strategy for Castrate-Resistant Prostate Cancer

5a. CONTRACT NUMBER
W81XWH-16-1-0562

5b. GRANT NUMBER

5c. PROGRAM ELEMENT NUMBER

6. AUTHOR(S)
Dr. Leonard Neckers
neckersl@nih.gov

5d. PROJECT NUMBER

5e. TASK NUMBER

5f. WORK UNIT NUMBER

7. PERFORMING ORGANIZATION NAME(S) AND ADDRESS(ES)
The Geneva Foundation
917 Pacific Ave. # 600
Tacoma, WA 98402

8. PERFORMING ORGANIZATION REPORT NUMBER

9. SPONSORING / MONITORING AGENCY NAME(S) AND ADDRESS(ES)
U.S. Army Medical Research and Development Command
Fort Detrick, Maryland 21702-5012

10. SPONSOR/MONITOR'S ACRONYM(S)

11. SPONSOR/MONITOR'S REPORT

12. DISTRIBUTION / AVAILABILITY STATEMENT
Approved for Public Release; Distribution Unlimited

13. SUPPLEMENTARY NOTES

14. ABSTRACT

Technical Abstract: Heat shock proteins Hsp40, Hsp70 and Hsp90 are molecular chaperones required for stabilization/activation of nuclear receptors, including full-length androgen receptor (AR) and glucocorticoid receptor (GR). Although ligandbinding domain (LBD) targeted (LBDT) therapy initially inhibits AR function and improves patient survival, this treatment almost invariably leads to emergence of castration-resistant prostate cancer (CRPC). CRPC is frequently characterized by elevated expression of alternative nuclear receptors able to at least partially maintain the AR transcriptional program. These alternative receptors include GR, which is expressed in approximately 30% of LBDT therapy-sensitive prostate cancer, but is expressed at a much higher frequency in CRPC and in those patients with a poor response to LBDT therapy. Additionally, elevated expression of a number of constitutively active AR splice variants lacking the LBD (ARv, particularly ARv7, which correlates with poor prognosis, reduced survival, and resistance to LBDT therapy, and ARv567es) is a frequent occurrence in CRPC. While full length GR and AR depend on the Hsp40/Hsp70/Hsp90 chaperone axis for activity, the chaperone requirements of ARv are not known. Because Hsp90 interacts with the LBD, ARv are insensitive to Hsp90 inhibitors. However, based on strong preliminary data, we believe that ARv, like GR and AR, retain dependence on Hsp40/Hsp70 and we will test this hypothesis using combined biophysical, genetic, biochemical and pharmacological approaches, including novel small molecules able to bind and inhibit both Hsp40 and Hsp70. We envision a synergistic group of studies that will result in a detailed and comprehensive picture of the specific chaperone dependence of these individual nuclear receptors. Together with in vivo xenograft data and with ex vivo evaluation of patient tumor biopsy tissue, we expect to obtain proof-of-principle confirmation that inhibition of Hsp40 and Hsp70 represents a novel strategy to target the continued nuclear receptor dependence of CRPC. Using in vitro and in vivo models, we will test whether this targeting strategy also can abrogate or delay onset of resistance in LBDT therapy-naïve patients.

Impact: The proposed research program is responsive to the goals and mission of the Depart of Defense Prostate Cancer Research Program (PCRP). Our proposal addresses the PCRP Overarching Challenge of developing effective treatments and mechanisms of resistance for men with high-risk or metastatic prostate cancer. Our proposal addresses the FY15 PCRP Focus Areas of (1) Mechanisms of Resistance and Response: Understanding primary and acquired resistance as well as exceptional response to therapy, and (2) Therapy: Identification of targets and pathways (Hsp40/Hsp70) and optimization (including sequencing and combination therapies of chaperone inhibitors) of therapeutic modalities, including metastatic prostate cancer.

15. SUBJECT TERMS
Cancer, Prostate Cancer, Oncology

16. SECURITY CLASSIFICATION OF:			17. LIMITATION OF ABSTRACT	18. NUMBER OF PAGES	19a. NAME OF RESPONSIBLE PERSON USAMRDC
a. REPORT	b. ABSTRACT	c. THIS PAGE			19b PHONE NUMBER *(include area code)*
Unclassified	Unclassified	Unclassified	Unclassified	39	

Table of Contents

1. INTRODUCTION: INTRODUCTION: Heat shock proteins Hsp40, Hsp70 and Hsp90 are molecular chaperones required for stabilization/activation of nuclear receptors, including full-length androgen receptor (AR) and glucocorticoid receptor (GR). Although ligand-binding domain (LBD) targeted (LBDT) therapy initially inhibits AR function and improves patient survival, this treatment almost invariably leads to emergence of castration-resistant prostate cancer (CRPC). CRPC is frequently characterized by elevated expression of alternative nuclear receptors able to at least partially maintain the AR transcriptional program. These alternative receptors include GR, which is expressed in approximately 30% of LBDT therapy-sensitive prostate cancer, but is expressed at a much higher frequency in CRPC and in those patients with a poor response to LBDT therapy. Additionally, elevated expression of a number of constitutively active AR splice variants lacking the LBD (ARv, particularly ARv7, which correlates with poor prognosis, reduced survival, and resistance to LBDT therapy, and ARv567es) is a frequent occurrence in CRPC. While full length GR and AR depend on the Hsp40/Hsp70/Hsp90 chaperone axis for activity, the chaperone requirements of ARv are not known. Because Hsp90 interacts with the LBD, ARv are insensitive to Hsp90 inhibitors. However, based on strong preliminary data, we believe that ARv, like GR and AR, retain dependence on Hsp40/Hsp70 and we will test this hypothesis using combined biophysical, genetic, biochemical and pharmacological approaches, including novel small molecules able to bind and inhibit both Hsp40 and Hsp70.

2. KEYWORDS: heat shock proteins, chaperones, protein-protein interactions, androgen receptor, androgen receptor splice variant, glucocorticoid receptor, proteostasis, chaperone inhibitors, protein turnover, degradation.

3. ACCOMPLISHMENTS:

What were the major goals of the project?

Specific Aims:

1. Using a combination of purified proteins, CRPC cells and cell lysates, we will identify the unique Hsp40/Hsp70 interactions with GR, AR and ARv and we will explore their functions(s).
2. Using CRPC cells, we will examine sensitivity of GR, AR & ARv to pharmacologic inhibition of the Hsp40/Hsp70 axis in vitro and resultant effects on xenograft growth in vivo.

What was accomplished under these goals? Most of the goals of SA1 were accomplished and data are included in a Cancer Research publication (Moses et al, 2018), provided and discussed in the 2018—2019 Annual Report. In the current cycle (NCE), we used a validated chaperone shRNA library, obtained from our collaborator Jason Gestwicki, to determine which of the closely related Hsp40 and Hsp70 paralogs, as well as additional proteostasis inhibiters are most important for nuclear receptor stability/function. These findings have been published (Arielle Shkedi, Michael Adkisson , Andrew Schroeder, Walter L Eckalbar, Szu-Yu Kuo, Leonard Neckers, Jason E Gestwicki. Inhibitor Combinations Reveal Wiring of the Proteostasis Network in Prostate Cancer Cells. J Med Chem, 2021, 64:14809-14821. doi:10.1021/acs.jmedchem.1c01342. PMID: 34606726 PMCID: PMC8806517 DOI: 10.1021/acs.jmedchem.1c01342) and are briefly summarized here. The protein homeostasis (proteostasis) network is composed of multiple

pathways that work together to balance protein folding, stability, and turnover. Cancer cells are particularly reliant on this network; however, it is hypothesized that inhibition of one node might lead to compensation. To better understand these connections, we dosed 22Rv1 prostate cancer cells with inhibitors of four proteostasis targets (Hsp70, Hsp90, proteasome, and p97), either alone or in binary combinations, and measured the effects on cell growth. Our data uncover a series of additive, synergistic, and antagonistic relationships, including strong synergy between inhibitors of p97 and the proteasome and striking antagonism between inhibitors of Hsp90 and the proteasome. Based on RNA-seq, these relationships are associated, in part, with activation of stress pathways. Together, these results suggest that cocktails of proteostasis inhibitors might be a powerful way of treating some CRPC, although antagonism that blunts the efficacy of both molecules is also possible. A second paper, performing functional and synthetic lethal screens in 4 PCa cell lines, also recently published (Arielle Shkedi, Isabelle R Taylor, Frank Echtenkamp, Poornima Ramkumar, Mohamed Alshalalfa, Génesis M Rivera-Márquez, Michael A Moses, Hao Shao, Robert Jeffrey Karnes, Len Neckers, Felix Feng, Martin Kampmann, Jason E Gestwicki. Selective vulnerabilities in the proteostasis network of castration-resistant prostate cancer. Cell Chem Biol. 2022; 29:490-501.e4. doi: 10.1016/j.chembiol.2022.01.008. Epub 2022 Feb 1. PMID: 35108506 PMCID: PMC8934263 (available on 2023-03-17) DOI: 10.1016/j.chembiol.2022.01.008), confirmed key roles for HSP70, HSP90, and their co-chaperones in supporting PCa viability, but the data also suggested that the mitochondrial chaperone, HSP60/HSPD1, is selectively required in CRPC cell lines. Knockdown of HSP60 did not impact the stability of androgen receptor (AR) or its variants; rather, it was associated with loss of mitochondrial spare respiratory capacity, partly owing to increased proton leakage. These findings suggest that re-wiring of the proteostasis network is associated with CRPC, creating selective vulnerabilities that might be targeted to treat the disease. Both published papers are appended at the end of this Annual Report.

The goals of SA2 have been partially accomplished. We validated the in vitro dependence of CRPC cells on Hsp70 interaction with full-length GR, AR and AR splice variants, as discussed in the previous Annual Report and as published in Cancer Research (Moses et al., 2018). However, due to technical difficulties that we had not fully appreciated, we were not able to complete the goal of determining whether Hsp40 and/or Hsp70 inhibitors could prevent or delay emergence of resistance to LBD-targeting therapy (including androgen synthesis inhibitors and androgen binding inhibitors). Instead, we re-focused this goal to determine whether inhibitors of one or both of these chaperones may synergize with standard of care inhibitors of androgen synthesis (abiraterone) and/or inhibitors of androgen binding to AR (enzalutamide). We have confirmed earlier preliminary in vitro data that demonstrate re-sensitization of CRPC to enzalutamide and abiraterone with the HSP70 inhibitor JG98 (see Fig. 1 on following page). During the upcoming cycle (NCE granted), in vivo animal studies (delayed because of Covid restrictions and papilloma virus contamination of our animal facility that necessitated an extensive quarantine and closure of the animal facility) will be performed and we hope to generate supporting animal xenograft data.

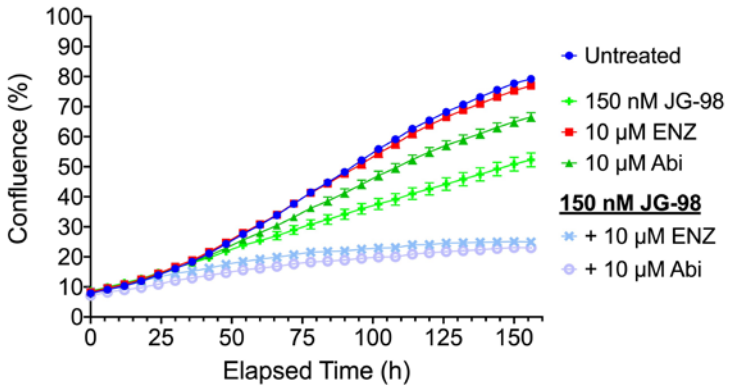

Figure 1. Intermediate concentration of HSP70 inhibitor JG98 re-sensitizes 22Rv1 CRPC cells in vitro to otherwise inactive concentrations of enzalutamide and abiraterone. Curves reflect viable cell growth in vitro over a 150-hour time period.

What opportunities for training and professional development did the project provide?
How were the results disseminated to communities of interest? Frank Echtenkamp joined the team as a senior postdoctoral fellow and received additional training in translational research. Dr. Echtenkamp has been promoted to Staff Scientist and is the lead on this study. Genesis Rivera-Marquez is currently a Geneva Foundation collaborator who continues work on the project while developing further expertise in molecular and cellular biology.

How were the results disseminated to communities of interest? In addition to the 2 published papers described above, results were disseminated via invited virtual seminars (e.g., lecture as part of the Proteostasis Consortium Virtual Seminar Series in July, 2021; lecture delivered at the CSSI XIth International Online Symposium on Heat Shock Proteins in Biology and Medicine, October 27-29, 2021, October 12, 2022).

What do you plan to do during the next reporting period to accomplish the goals and objectives? We plan to complete the in vivo CRPC xenograft studies described in SA2.

4. IMPACT:

What was the impact on the development of the principal discipline(s) of the project? The molecular chaperones Hsp40 and Hsp70 were shown to interact with the NTD (N-terminal domain) of glucocorticoid receptors (GR) and androgen receptors (AR) and thus were shown to interact with both full-length GR and AR, and with constitutively active AR splice variants retaining the NTD but lacking the ligand binding domain. Likewise, both full-length GR, AR and AR splice variants were shown to be destabilized at the protein level by inhibitors of Hsp40 and Hsp70. In vitro transcriptional activity of full-length GR, AR and AR splice variants was shown to be inhibited. Inhibitors of these chaperones, both singly and combined, displayed in vivo anti-tumor activity in prostate cancer xenografts resistant to standard of care therapy targeting both androgen synthesis and androgen binding to AR. Thus, we demonstrated that chaperone inhibitor targeting of nuclear receptor NTD may represent a novel treatment strategy for CRPC. Unexpectedly, we also found that that the mitochondrial chaperone, HSP60/HSPD1, is selectively required ifor viability in CRPC cell lines. Knockdown of HSP60 did not impact the stability of androgen receptor (AR) or its variants; rather, it was associated with loss of mitochondrial spare respiratory capacity, partly owing to increased proton leakage. These findings suggest that re-wiring of the proteostasis network is associated with CRPC, creating selective vulnerabilities that might be targeted to treat the disease.

What was the impact on other disciplines? Nothing to Report.

What was the impact on technology transfer? Nothing to Report.

What was the impact on society beyond science and technology? Nothing to Report.

5. CHANGES/PROBLEMS: Nothing to report other than what is described above.

Changes in approach and reasons for change
Nothing to Report.

Actual or anticipated problems or delays and actions or plans to resolve them:
Nothing to Report.

Changes that had a significant impact on expenditures
Nothing to Report.

Significant changes in use or care of human subjects, vertebrate animals, biohazards, and/or select agents:
Nothing to Report.

Significant changes in use or care of human subjects:
N/A

Significant changes in use or care of vertebrate animals:
Nothing to Report.

Significant changes in use of biohazards and/or select agents:
Nothing to Report.

6. PRODUCTS:

Publications, conference papers, and presentations
Invited lecture as part of the Proteostasis Consortium Virtual Seminar Series in July, 2021; Invited lecture delivered at the CSSI XIth International Online Symposium on Heat Shock Proteins in Biology and Medicine, October 27-29, 2021, October 12, 2022

Journal publications: Arielle Shkedi, Michael Adkisson , Andrew Schroeder, Walter L Eckalbar, Szu-Yu Kuo, Leonard Neckers, Jason E Gestwicki. Inhibitor Combinations Reveal Wiring of the Proteostasis Network in Prostate Cancer Cells. J Med Chem, 2021, 64:14809-14821. doi:10.1021/acs.jmedchem.1c01342. PMID: 34606726 PMCID: PMC8806517 DOI: 10.1021/acs.jmedchem.1c01342 (federal support is acknowledged)

Arielle Shkedi, Isabelle R Taylor, Frank Echtenkamp, Poornima Ramkumar, Mohamed Alshalalfa, Génesis M Rivera-Márquez, Michael A Moses, Hao Shao, Robert Jeffrey Karnes, Len Neckers, Felix Feng, Martin Kampmann, Jason E Gestwicki. Selective vulnerabilities in the proteostasis network of castration-resistant prostate cancer. Cell Chem Biol. 2022; 29:490-

501.e4. doi: 10.1016/j.chembiol.2022.01.008. Epub 2022 Feb 1. PMID: 35108506 PMCID: PMC8934263 (available on 2023-03-17) DOI: 10.1016/j.chembiol.2022.01.008 (federal support is acknowledged)

Books or other non-periodical, one-time publications:
Nothing to Report

Other publications, conference papers, and presentations:
Nothing to Report

Website(s) or other Internet site(s):
Nothing to Report

Technologies or techniques:
Nothing to Report

Inventions, patent applications, and/or licenses:
Nothing to Report

Other Products:
Nothing to Report

7. PARTICIPANTS & OTHER COLLABORATING ORGANIZATIONS:

Name:	Len Neckers
Project Role:	No change
Researcher Identifier (e.g. ORCID ID):	
Nearest person month worked:	No change
Contribution to Project:	No change
Funding Support:	No change

Name:	Jane Trepel
Project Role:	No change

Researcher Identifier (e.g. ORCID ID):	
Nearest person month worked:	No change
Contribution to Project:	No change
Funding Support:	No change

Has there been a change in the active other support of the PD/PI(s) or senior/key personnel since the last reporting period?
Nothing to Report

What other organizations were involved as partners?
Nothing to Report

8. SPECIAL REPORTING REQUIREMENTS:
N/A

9. APPENDICES:
Two manuscript reprints (PDFs) described above are attached.

Journal of Medicinal Chemistry

pubs.acs.org/jmc

Article

Inhibitor Combinations Reveal Wiring of the Proteostasis Network in Prostate Cancer Cells

Arielle Shkedi, Michael Adkisson, Andrew Schroeder, Walter L Eckalbar, Szu-Yu Kuo, Leonard Neckers, and Jason E. Gestwicki*

Cite This: *J. Med. Chem.* 2021, 64, 14809−14821

Read Online

ACCESS | Metrics & More | Article Recommendations | Supporting Information

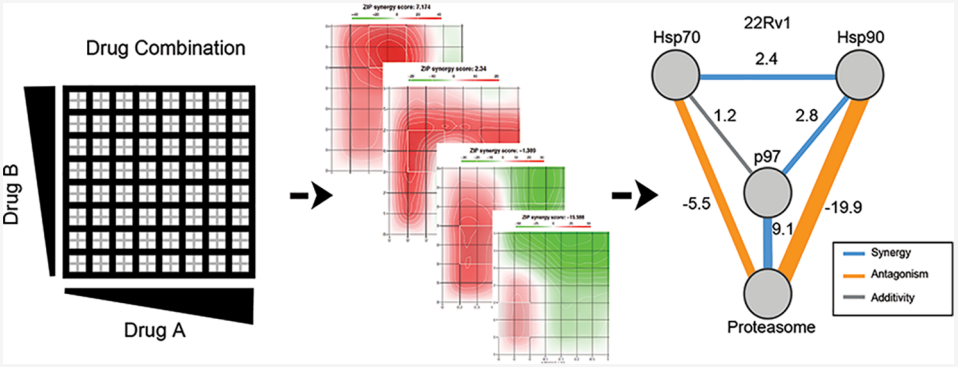

ABSTRACT: The protein homeostasis (proteostasis) network is composed of multiple pathways that work together to balance protein folding, stability, and turnover. Cancer cells are particularly reliant on this network; however, it is hypothesized that inhibition of one node might lead to compensation. To better understand these connections, we dosed 22Rv1 prostate cancer cells with inhibitors of four proteostasis targets (Hsp70, Hsp90, proteasome, and p97), either alone or in binary combinations, and measured the effects on cell growth. The results reveal a series of additive, synergistic, and antagonistic relationships, including strong synergy between inhibitors of p97 and the proteasome and striking antagonism between inhibitors of Hsp90 and the proteasome. Based on RNA-seq, these relationships are associated, in part, with activation of stress pathways. Together, these results suggest that cocktails of proteostasis inhibitors might be a powerful way of treating some cancers, although antagonism that blunts the efficacy of both molecules is also possible.

INTRODUCTION

The proteostasis network is a highly conserved set of pathways that balances the synthesis, folding, activation, and degradation of the proteome.[1] There are hundreds of components dedicated to this network, including molecular chaperones (*e.g.,* heat shock proteins), co-chaperones, the translation machinery, the ubiquitin−proteasome system, and the autophagy−lysosome pathway.[2,3] This network is characterized by major "nodes" that are connected, often through direct protein−protein interactions, with the other components.[4] Importantly, the flux of proteins through this network is tightly regulated by stress signaling, including the unfolded protein response (UPR), the integrated stress response (ISR), the heat shock response (HSR), and others.[5−8] Specifically, stress signaling often elevates the levels of proteostasis factors, such as some chaperones, as well as tuning the rates of protein synthesis and turnover, allowing cells to adapt to changing conditions. Thus, the proteostasis network is both interconnected and responsive, likely allowing different subnetworks to play dominant roles in response to specific perturbations.[9]

Cancer cells have been found to be particularly reliant on specific components of the proteostasis network, likely because of the rapid growth, high frequency of translation errors, and genomic instability of these cells.[10,11] For example, major nodes of the proteostasis network, such as Hsp70, Hsp90, and HSF1, are important for maintaining tumorigenesis.[7,12,13] In contrast, normal, untransformed cells seem to be less reliant on these same proteostasis factors, perhaps because their networks are more robust to the loss of an individual component. The mechanistic reasons for differential vulnerability are often not clear, but recent studies have started to provide insights. For

Received: August 2, 2021
Published: October 4, 2021

https://doi.org/10.1021/acs.jmedchem.1c01342
J. Med. Chem. 2021, 64, 14809−14821

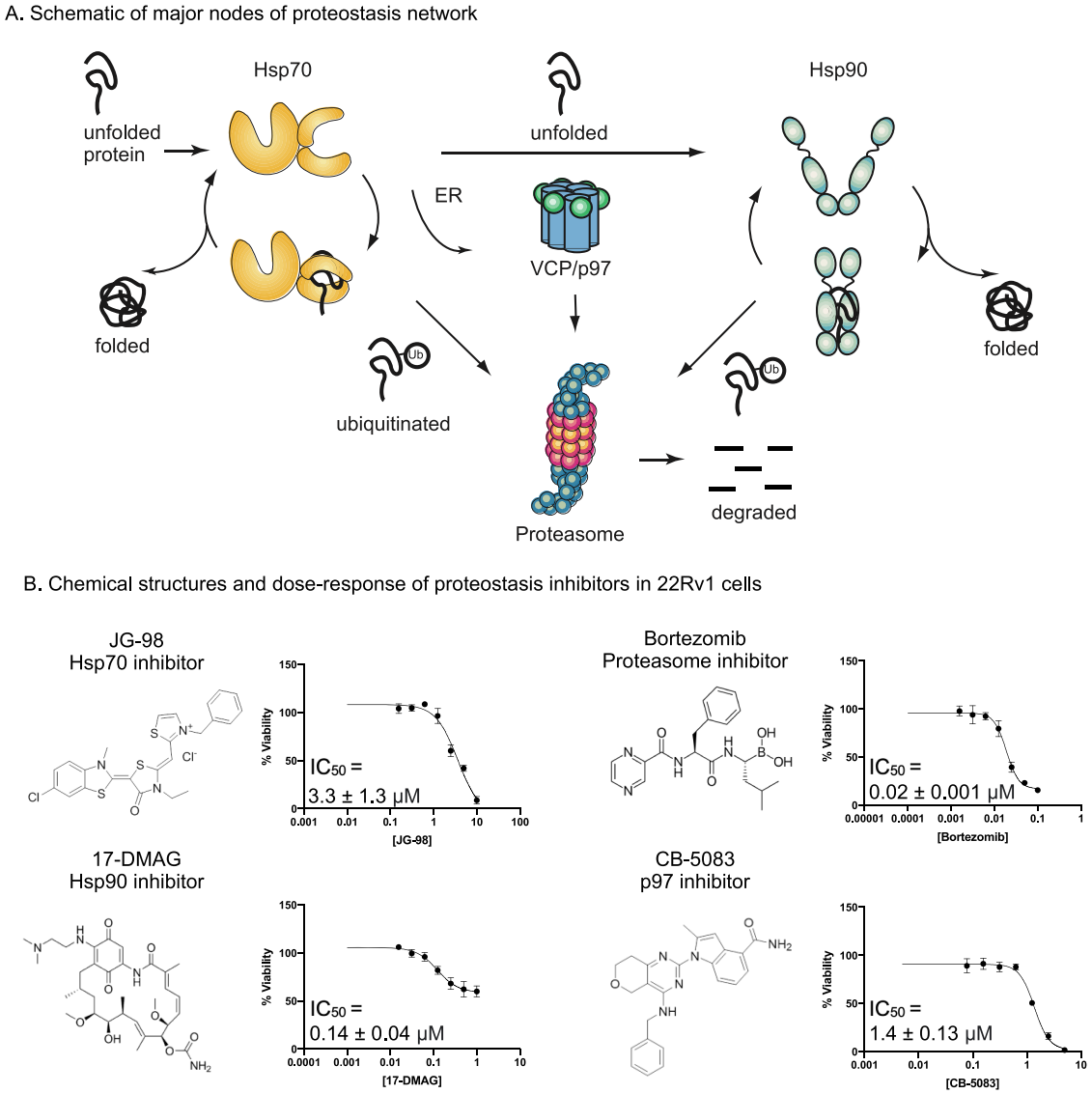

Figure 1. Proteostasis inhibitors, targeting multiple nodes of the proteostasis network, have antiproliferative effects in 22Rv1 prostate cancer cells. (A) Subset of the proteostasis network is shown, highlighting the connections between the major nodes: Hsp70, Hsp90, p97, and the proteasome. Together, these factors guide protein folding and turnover, working together to mediate client "hand-off". (B) Inhibitors of proteostasis nodes limit the growth of 22Rv1 cells. In this study, four inhibitors were used: JG-98 (Hsp70 inhibitor), 17-DMAG (Hsp90 inhibitor), bortezomib (proteasome inhibitor), and CB-5083 (p97 inhibitor). Cells were incubated with the indicated compound for 72 h, and viability was measured via Cell Titer Glo (see the methods section). Results are the average of experiments performed in quadruplicate and the error bars represent SD. Some error bars are smaller than symbols.

example, Hsp90 binds to a distinct set of co-chaperones in cancer cells vs non-transformed cells,[14,15] suggesting that the same node can be "wired" differently following tumorigenesis.

These observations, and others, have led to the hypothesis that nodes of the proteostasis network are promising drug targets, which could be exploited for anticancer therapy.[16−19] Accordingly, substantial efforts have been mobilized to create chemical inhibitors of proteostasis targets.[20−22] Although this remains as an active research area, a subset of these molecules has advanced to the clinical setting, with varying levels of success. For example, proteasome inhibitors are approved and widely used in treating multiple myeloma.[23] However, inhibitors of other proteostasis targets have been less successful,[24−26] often due to lack of efficacy, rapid onset of resistance, and/or unacceptable toxicity. Moreover, even proteasome inhibitors are ineffective at treating some cancer subtypes, such as solid tumors, for reasons that remain uncertain.[27]

One hypothesis to explain the uneven and sometimes confounding clinical results is that the interconnected nature of the proteostasis network might create opportunities for compensation by stress responses.[28] For example, it is well established that treatment with Hsp90 inhibitors, at least those that bind the N-terminal domain, leads to elevated expression of Hsp70 and other chaperones via an HSR program.[10] Similarly, proteasome inhibitors induce autophagy pathways,[29] and inhibition of p97 activates the UPR.[22] Mounting evidence suggests that these compound-induced stress responses might directly contribute to inhibitor resistance. For example, activation of autophagy and other stress pathways[28] makes certain cancer cells relatively resistant to Hsp70 inhibition.[30] Additionally, activation of the HSR has been linked to

https://doi.org/10.1021/acs.jmedchem.1c01342
J. Med. Chem. 2021, 64, 14809−14821

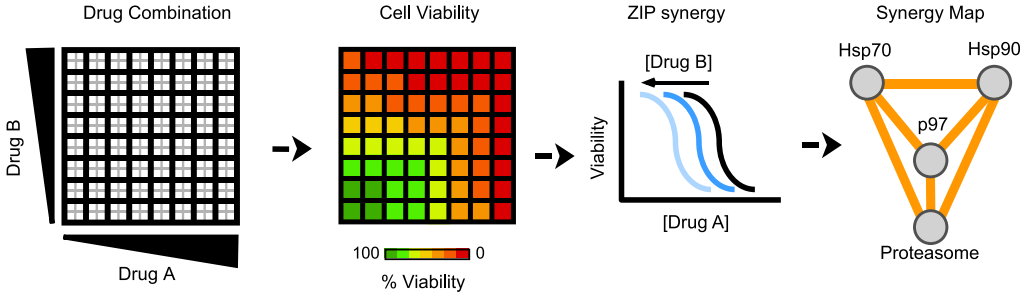

Figure 2. Workflow for the measurement of additivity, synergy, or antagonism amongst proteostasis inhibitors. Briefly, cells are aliquoted to 384-well plates and allowed to adhere for 1 day. Then, two drugs (A, B) are added in an 8×8 matrix format, with 7 doses per compound, using twofold dilutions (see the methods for tested concentrations) and a DMSO solvent control. Treatments were performed in quadruplicate, with 4 wells per each dose combination (gray squares). After 72 h of treatment, cell viability was measured using Cell Titer Glo, and synergy was determined through the ZIP synergy model. Drug-combination screens were performed twice per cell line, and the ZIP synergy score was averaged between replicates. Under this model, addition of Drug B reducing the potency of Drug A (blue lines) would be considered synergy. ZIP scores around zero (between 1.5 and −1.5) were considered additive, while scores above 1.5 were considered synergistic and those below −1.5 were considered antagonistic. To map these relationships onto the proteostasis subnetwork (see Figure 1A), we plotted the nodes and created lines between them to indicate whether the ZIP synergy score was additive, synergistic, or antagonistic for each tested cell line (termed a synergy map).

bortezomib resistance in multiple myeloma.[31,32] Thus, cancer cells seem to activate stress pathways in response to proteostasis inhibitors, which can, in some cases, provide them with partial protection.

Because the nodes of the proteostasis network are interconnected and subject to regulation by stress responses, combinations of proteostasis inhibitors might, in some cases, be strongly synergistic.[33] Specifically, inhibition of two proteostasis targets simultaneously might limit the ability of cancer cells to circumvent loss of one target. However, while some promising combinations have been proposed,[34−36] this possibility has not been systematically explored. Here, we tested four proteostasis inhibitors by themselves and in binary combinations to reveal additive, synergistic, and antagonistic relationships. We chose to perform these screens in 22Rv1 prostate cancer cells, given the known reliance of these cells on the proteostasis network.[37,38] As test compounds, we selected four well-known inhibitors that target major nodes in the proteostasis network: Hsp70, Hsp90, the 26S proteasome, and VCP/p97. Briefly, Hsp70 and Hsp90 are molecular chaperones involved in protein folding and activation.[39] VCP/p97 is a AAA^+ ATPase that plays multiple roles in protein trafficking and quality control,[40] and the 26S proteasome is responsible for degrading ubiquitinated proteins.[41] Beyond their individual functions, these nodes also engage in functional relationships within a defined subnetwork (Figure 1A). For example, Hsp70 delivers unfolded proteins to Hsp90 through a shared co-chaperone, HOP.[42,43] Moreover, p97 collaborates with Hsp70 and the proteasome during endoplasmic reticulum (ER)-associated degradation (ERAD)[44,45] and both Hsp70 and Hsp90 are involved in delivering proteins to the proteasome for degradation.[46,47] Thus, we were interested in whether an inhibitor of one node in this particular subnetwork might create synergy with inhibitors of others.

To target these four nodes, we selected well-characterized chemical inhibitors: JG-98 (Hsp70 inhibitor),[48] 17-DMAG (Hsp90 inhibitor),[49] bortezomib (proteasome inhibitor),[50] and CB-5083 (p97 inhibitor)[22] (Figure 1B). These compounds were selected because three of them have been explored in clinical trials, while the fourth, JG-98, is a close analog of a molecule, MKT-077, tested in Phase I.[51] Using a high throughput, 384-well growth assay, we tested binary combinations of the compounds on the growth of 22Rv1 prostate cancer cells, revealing examples of both synergy (Hsp70-Hsp90, p97-Hsp90, and p97-proteasome) and antagonism (Hsp70-proteasome and Hsp90-proteasome). Transcriptome studies on cells treated with the most promising combinations revealed differences in the cellular stress response(s) compared to the single-agent treatments, perhaps underlying, in part, the observed relationships. Also, repeating these screens in three additional prostate cancer cell lines, C4-2, LNCaP, and PC3, identified both shared and cell-type specific relationships, suggesting that the "wiring" of the proteostasis network can partially differ across cell lines. Together, these studies show that testing proteostasis inhibitor combinations in cultured cells reveals patterns of additivity, synergy, and antagonism, which could aid in the design (or avoidance) of therapeutic combinations for use in the clinic.

RESULTS

Proteostasis Inhibitors Reduce Cell Viability in 22Rv1 Prostate Cancer Cells, as Single Agents. To provide a baseline for combination studies, we first confirmed the effects of the four proteostasis inhibitors, JG-98 (Hsp70 inhibitor), 17-DMAG (Hsp90 inhibitor), bortezomib (proteasome inhibitor), and CB-5083 (p97 inhibitor), on the growth of 22Rv1 cells as single agents. After a 72 h treatment, each of the inhibitors, but not the DMSO control, reduced the growth of 22Rv1 cells, with IC_{50} values varying from 0.02 to 3.3 μM (Figure 1B). Consistent with observations from the literature, inhibitors of Hsp70, p97, and the proteasome reduced cell viability to nearly the baseline at the highest doses, while Hsp90 inhibition produced ∼50% reduction, even at the highest concentrations.

Combination Treatments Reveal Patterns of Additivity, Synergy, and Antagonism upon Proteostasis Disruption. Based on the calculated IC_{50} values, we then chose compound concentration ranges for use in the combination screens (see the methods section). First, 22Rv1 cells were plated in 384-well plates, and on the following day, compounds were added using standard laboratory automation. Treatments were performed in quadruplicate (4 wells per treatment), and each compound was tested in eight concentrations (DMSO control, plus 7 doses in twofold dilutions; Figure 2). After 3 days of treatment, cell viability was quantified using Cell Titer Glo. From the resulting data, all of

https://doi.org/10.1021/acs.jmedchem.1c01342
J. Med. Chem. 2021, 64, 14809−14821

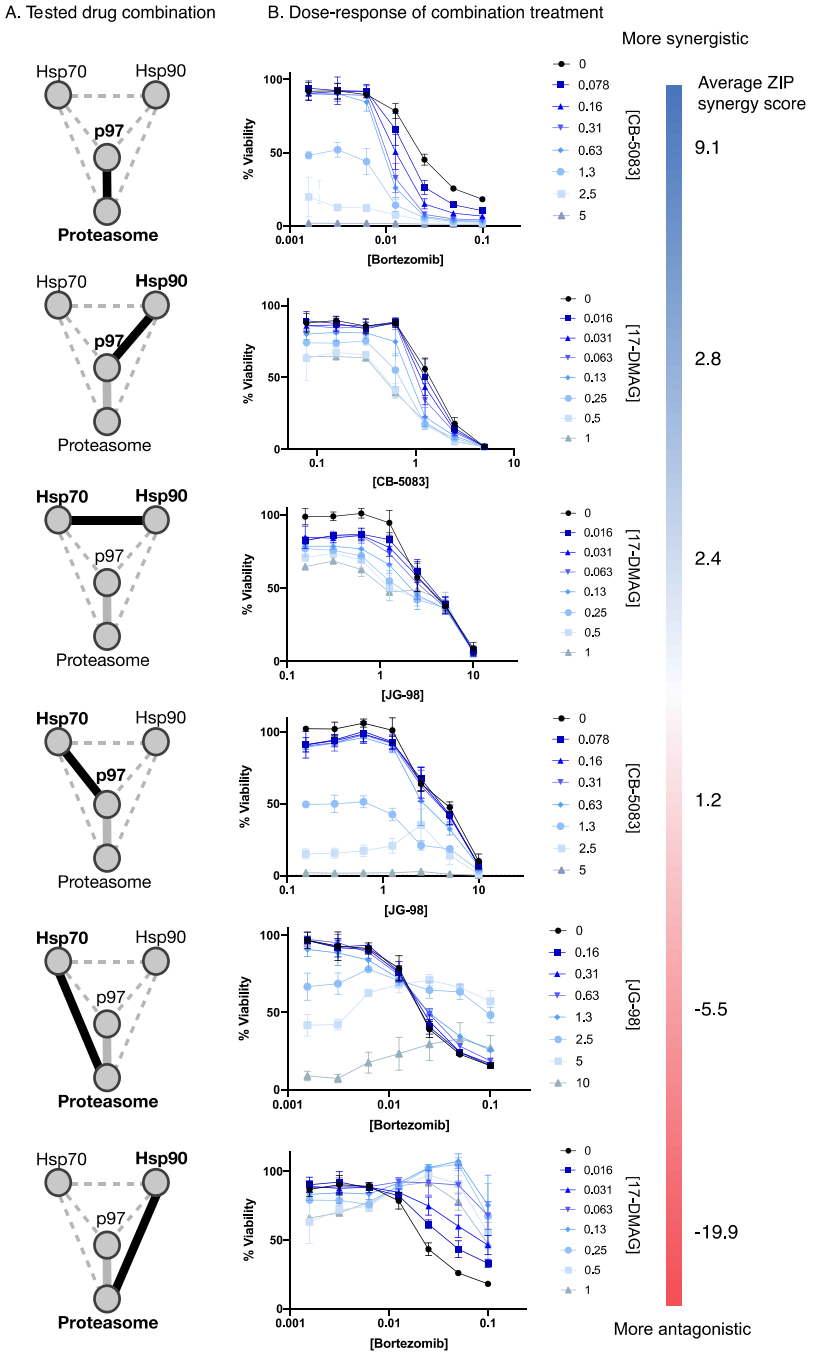

Figure 3. Combinations were either additive, synergistic, or antagonistic in 22Rv1 cells. (A) For each combination, a black line and bolded text indicates the tested nodes on the synergy map in the highlighted adjacent dose−response panel. (B) Dose−response curves from each combination are used to highlight additivity, synergy, or antagonism. In each graph, the single-agent (black) and combination treatments (blue curves) are shown. Curves are arranged from top to bottom from the most synergistic to the most antagonistic, with the average ZIP synergy scores shown. For the full matrix viability and synergy results, see Figure S1. All concentrations are in micromolar.

the values in the 8×8 treatment matrix were used to calculate synergy values using the ZIP synergy model[52] (Figure 2). There are multiple methods for estimating potential synergy or antagonism between compounds[53,54] and consensus in which approach to select has been elusive.[55,56] In this case, we chose to use ZIP synergy because it utilizes the entire dose−response landscape (Figure 2 and Figure S1), ensuring that all of the doses are represented when determining the numerical synergy value. This feature was especially important here because the Hsp90 inhibitor 17-DMAG did not reduce viability to baseline, which we found could create misleading synergy values if other approaches were employed. In this study, we considered scores to be additive if they were between the values of +1.5 and −1.5, while scores greater than +1.5 were categorized as synergistic and those less than −1.5 were antagonistic. We arrived at these arbitrary cutoff values by comparing the variance of the ZIP synergy scores across replicates and by manually examining the dose−response curves (see below). Importantly, this protocol and analysis pipeline was reprodu-

https://doi.org/10.1021/acs.jmedchem.1c01342
J. Med. Chem. 2021, 64, 14809−14821

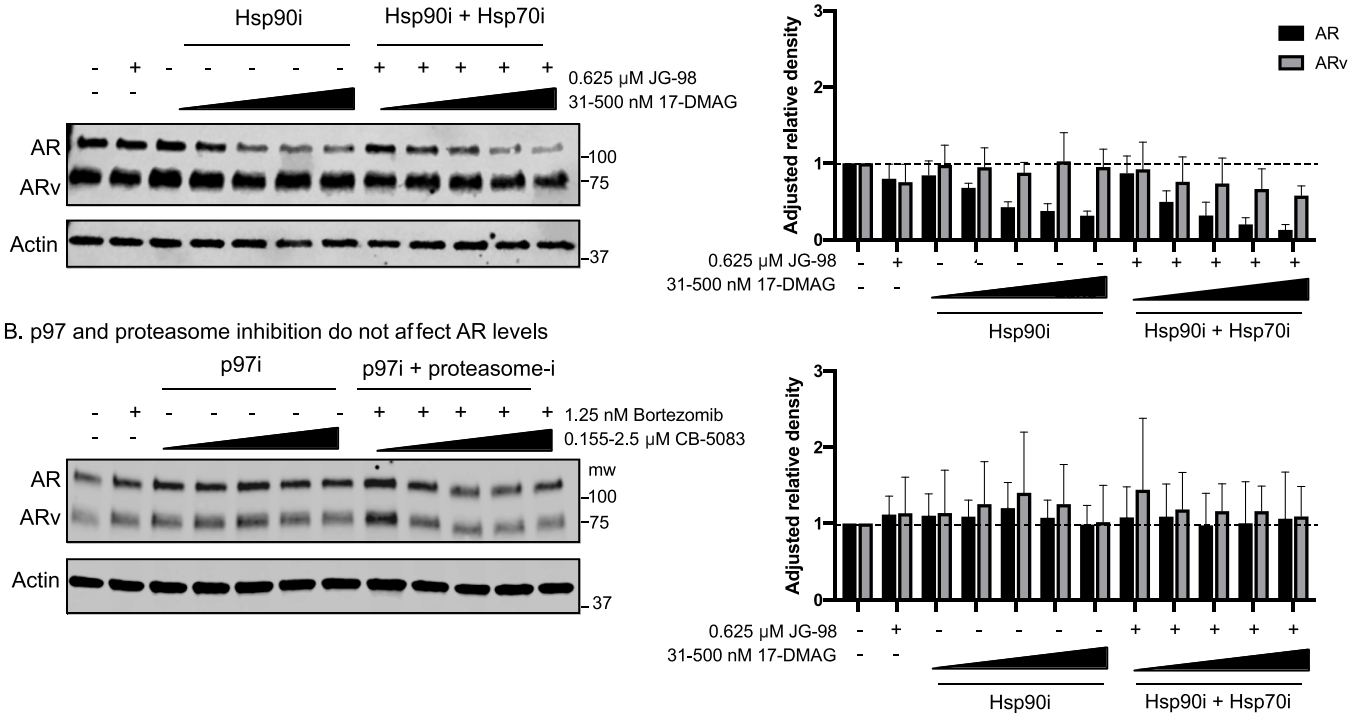

Figure 4. Some combinations reduce androgen receptor levels, but others do not. The effects of proteostasis inhibitor combinations on AR levels in 22Rv1 cells following 6 h treatment. (A) Treatment with the Hsp90 inhibitor 17-DMAG reduces the levels of full length AR, and Hsp70 inhibitor JG-98 treatment reduces levels of both AR and ARv in 22Rv1 cells after 6 h. The combination was effective at reducing both proteins. (B) Neither the p97 nor proteasome inhibitor, or their combination, had an effect on AR or ARv levels at 6 h. Western blots are representative of three independent experiments. The blots were quantified in NIH ImageJ, and the average density adjusted to the loading control and DMSO treatment was plotted on the right. Error bars represent SD.

cible, with independent replicates on different days showing high correlation (Figure S1).

From the combination screens in 22Rv1 cells, we observed clear patterns of additivity, synergy, and antagonism between the proteostasis inhibitors. For example, the combination of Hsp70 and p97 inhibitors was additive (ZIP score of ∼1.2), as co-treatment with the p97 inhibitor did not significantly impact the apparent IC_{50} of the Hsp70 inhibitor (Figure 3). However, other combinations, such as Hsp90-p97, Hsp90-Hsp70, and proteasome-p97, were found to be synergistic. The combinations of Hsp90-p97 and Hsp70-Hsp90 were modestly synergistic (ZIP scores between +2.4 and +2.8), while the combination of p97 and the proteasome inhibitor (compounds bortezomib and CB-5083) was the most strongly synergistic, with a ZIP score of +9.1. This relationship is illustrated by examining a subset of the dose−response curves, in which bortezomib alone is able to decrease cell viability (Figure 3; black curve), but the apparent IC_{50} is enhanced when CB-5083 is added (Figure 3; blue curves). These findings of strong synergy confirm the long-standing idea that targeting two proteostasis nodes might, in some cases, enhance cancer cell death.

In addition to synergistic combinations, we were surprised to observe combinations that were antagonistic. For example, the Hsp70-proteasome combination was moderately antagonistic (ZIP score, −5.5). This effect seemed most prominent at the higher doses of the Hsp70 inhibitor, as is clear from an examination of dose−response curves that show how the proteasome inhibitor (Figure 3; black curves) becomes less effective when the cells are also dosed with an Hsp70 inhibitor (Figure 3; blue curves). More strikingly, we found that the combination of Hsp90 and proteasome inhibitors was strongly antagonistic (ZIP score, −19.9). In a representative series of results, addition of 17-DMAG (Figure 3; blue curves) clearly suppresses the antiproliferative activity of bortezomib compared to this compound alone (Figure 3; black curve). Indeed, at the higher doses of the Hsp90 inhibitor, the antiproliferative effects of the proteasome inhibitor are nearly abolished. Thus, some proteostasis combinations can be strongly antagonistic.

To provide additional insight, we repeated a subset of the combination treatments, replacing 17-DMAG for an alternative Hsp90 inhibitor, AUY-922. In those studies, we observed effects consistent with those obtained using 17-DMAG (Figure S2A), suggesting that antiproliferative activities are, at least in part, a product of target biology and not specific to the compound. Next, we repeated the screens using a non-tumorigenic prostate cell line RWPE-1 and found no strong synergy between any drug combinations (Figure S2B). Thus, the combinations did not seem to generally increase toxicity to cells but rather enhance selectivity for 22Rv1 cancer cells over the non-tumorigenic cells. Finally, we wanted to ensure that the handling steps do not contribute to the observed synergy values, so we repeated the combinations by testing compounds against themselves. In those studies, we found no synergy or antagonism (Figure S2C), giving additional confidence in the screening platform.

Androgen Receptor (AR) Stability May Explain Some, but Not All, Drug Synergies. We next wanted to explore possible mechanisms of synergy and/or antagonism. 22Rv1

https://doi.org/10.1021/acs.jmedchem.1c01342
J. Med. Chem. 2021, 64, 14809−14821

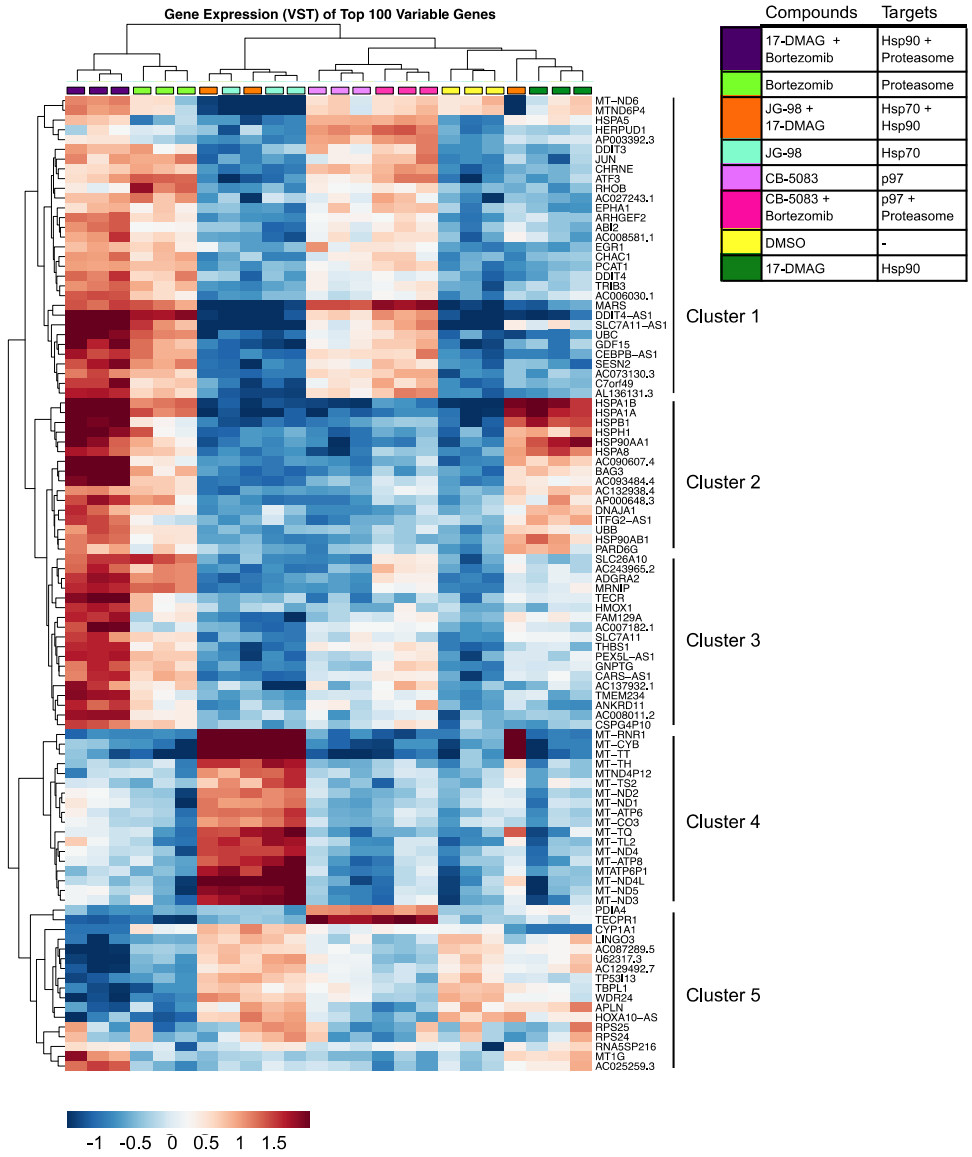

Figure 5. RNA-Seq data highlight differences in gene expression following single-agent and combination proteostasis inhibitor treatments. 22Rv1 cells were treated with the indicated compounds for 6 h, after which RNA-seq was performed (see the methods section). The top 100 variably expressed genes across all combinations were clustered and further analyzed.

cells are a prostate cancer cell line that is reliant on androgen receptor (AR) signaling.[57] However, these cells are relatively resistant to anti-androgen therapy because they express both full length (FL) AR and androgen-independent splicing variants (ARv) associated with severe diseases.[58] AR and its variants are established clients of Hsp70 and Hsp90,[37] and inhibitors of these chaperones have been shown to promote degradation of AR and ARv.[37,59] Indeed, we confirmed that treatment with combinations of JG-98 and 17-DMAG leads to loss of FL and ARv in 22Rv1 cells (Figure 4A), reducing AR to ∼10% of the total and ARv to ∼60% of the total. Consistent with previous reports,[37] the single-agent treatments show that Hsp70 inhibition has a more dramatic effect on ARv, while Hsp90 inhibition preferentially destabilizes FL AR. Thus, Hsp70 and Hsp90 inhibitors may be synergistic because their co-treatment leads to lower levels of both AR and ARv, interrupting the AR signaling required for the growth of these cells. However, AR stability did not explain all of the synergies. For example, treatment with the synergistic combination, p97-proteasome, did not alter either AR or ARv levels under the same conditions (Figure 4B). Likewise, AR stability did not correlate with synergy or antagonism after co-treatment with inhibitors of p97-Hsp70, Hsp70-proteasome, or Hsp90-proteasome (Figure S3), as there was no substantial differences between single-agent and combination treatments. Together, these results suggest that AR stability can be important but that different mechanism(s) may be underlying drug synergy and antagonism in response to most of the combinations.

RNA-Seq Experiments Reveal Differential Activation of Stress Responses that Occur after Treatment with Inhibitor Combinations. To examine the downstream effects of proteostasis inhibition in an unbiased way, RNA-seq was used to identify transcriptional differences in the response of 22Rv1 cells to compounds and their combinations. Based on the growth assays, we focused these studies on eight treatment conditions: a DMSO control, Hsp70, Hsp90, p97, or proteasome inhibition alone and the Hsp70-Hsp90, p97-proteasome, and Hsp90-proteasome combinations. These

https://doi.org/10.1021/acs.jmedchem.1c01342
J. Med. Chem. 2021, 64, 14809−14821

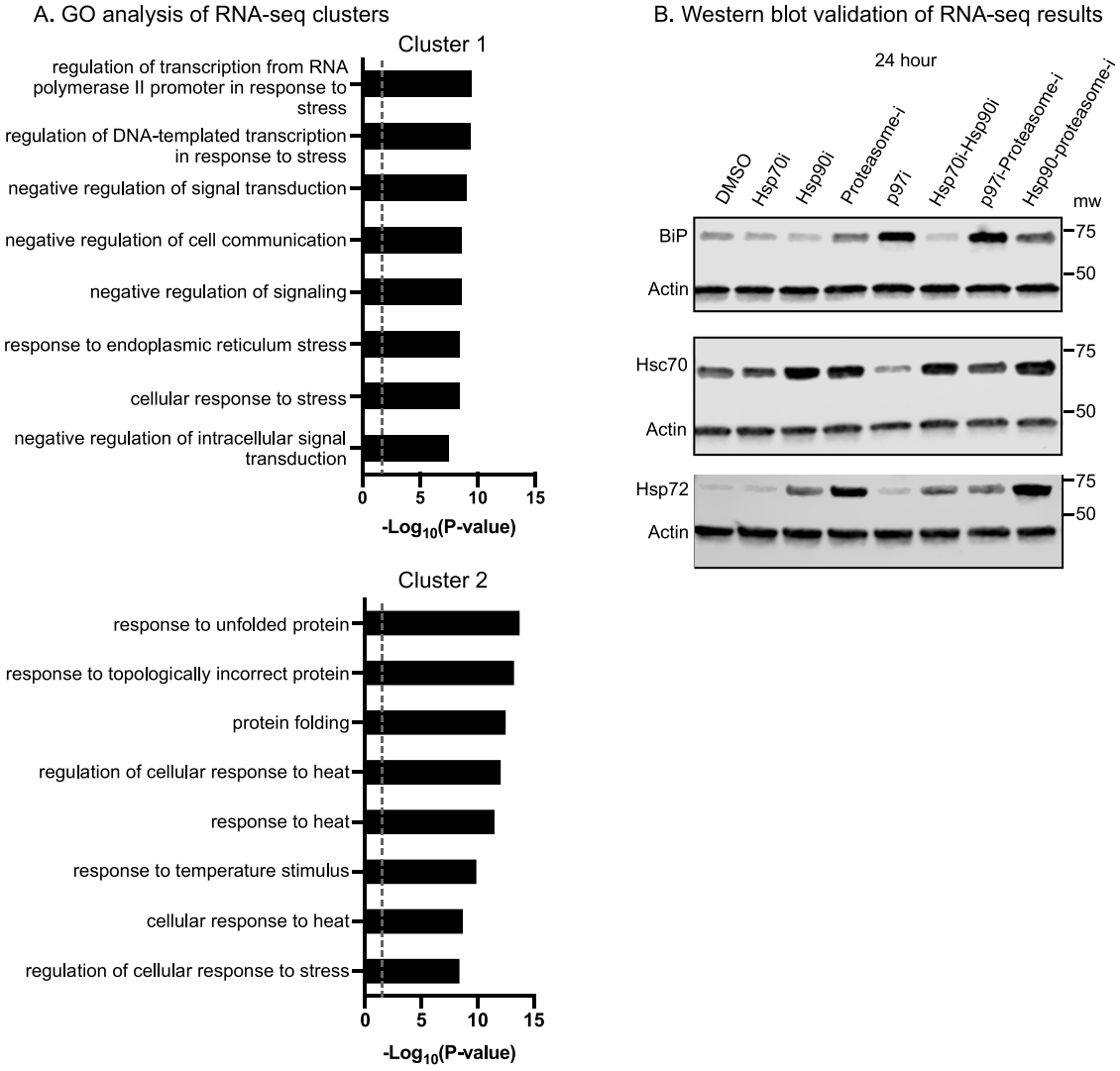

Figure 6. RNA-Seq studies and protein level validation highlight differences in activation of stress response pathways between single-agent and combination proteostasis inhibitor treatments. (A) Gene ontology (GO) analysis of clusters 1 and 2 from top variably expressed genes (see Figure 5). The top 8 most significantly enriched GO terms are shown. (B) BiP, Hsc70, and Hsp72 levels were probed via Western blot following 24 h of compound treatment (see the methods' section for the concentrations used). Protein levels at 24 h closely match transcriptomic data and are differentially expressed across single-agent and combination proteostasis inhibition. Results are representative of three independent experiments.

combinations were selected to sample both synergistic (Hsp70-Hsp90 and p97-proteasome) and antagonistic (Hsp90-proteasome) examples. In the RNA-seq studies, compounds were tested at a single concentration, selected by considering both the IC_{50} values (see Figure 1) and the results from the ZIP synergy analysis (see the methods section).

22Rv1 cells were treated for 6 h with the indicated compounds in triplicate, after which RNA was extracted and RNA-seq was performed (see the methods section). Read count data was analyzed by DeSeq2 and the top 100 variably expressed genes were hierarchically clustered and visualized (Figure 5). First, we noted that almost all of the biological replicates clustered together, suggesting a reproducible and specific transcriptional response to each treatment. The only outlier was the combination of JG-98 (Hsp70 inhibitor) and 17-DMAG (Hsp90 inhibitor), where one of the three replicates did not immediately co-cluster. Next, we further subdivided the top 100 variably expressed genes across all the treatments into five clusters (clusters 1−5) and examined them via gene ontology (GO) analysis (Figure 6A). Cluster 1 contains stress response genes, such as DDIT4 and SESN2, as well as ER stress response genes linked to the UPR, including HSPA5 (BiP, an ER Hsp70) and DDIT3 (CHOP). Cluster 2 contains many heat shock proteins and co-chaperones, including multiple Hsp70s (HSPA1B, HSPA1A, HSPB1, HSPH1, and HSPA8), Hsp90s (HSP9-AA1 and HSP90AB1), Hsp70 co-chaperones (DNAJA1 and BAG3), and ubiquitin (UBB). These genes are known to be upregulated following Hsp90 inhibition, but we additionally found that this effect is exacerbated by the combined Hsp90-proteasome inhibition (Figure 5). Qualitatively, this group of genes includes many hallmarks of the HSR.[60] Clusters 3 and 5 produced less well-defined GO terms, and their relevance will require an additional study. However, we were interested to find that cluster 4 contains exclusively mitochondrially expressed genes (Figure 5). The mitochondrial genome contains 37 genes, and we observed upregulation of a significant portion following treatment with either JG-98 alone or the JG-98 and 17-DMAG combination. JG-98 has

https://doi.org/10.1021/acs.jmedchem.1c01342
J. Med. Chem. 2021, 64, 14809−14821

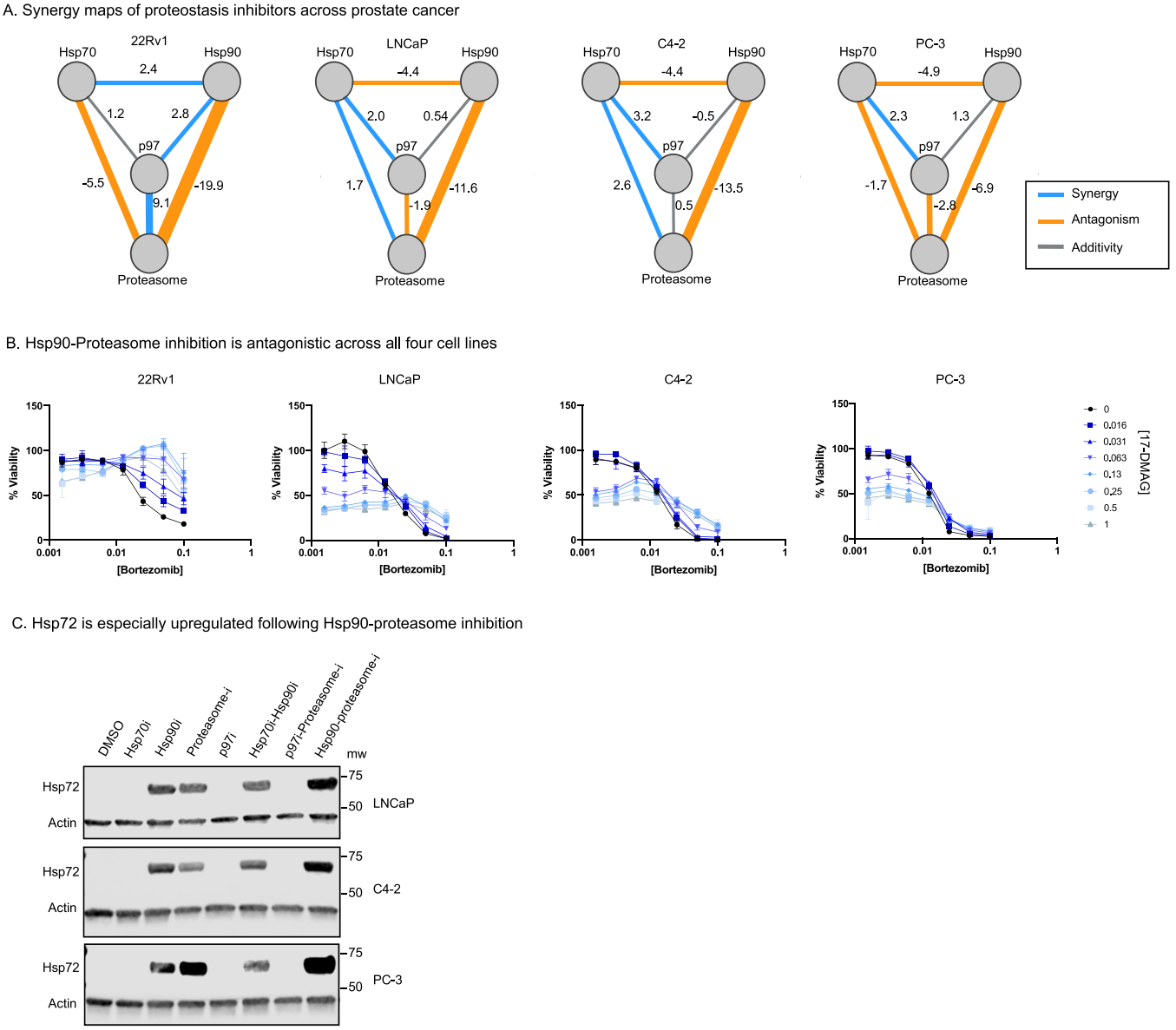

Figure 7. Expanded screens in additional prostate cancer cell lines reveal both similarities and differences in their responses to combinations of proteostasis inhibitor treatment. (A) Synergy maps depicting the relationship between proteostasis nodes from the drug-combination screens. Synergy is blue, antagonism is orange, and additivity is gray. Cutoffs defined in Figure 2 were applied here. Screens were performed as described in Figure 2, with each dose combination performed in quadruplicate. Each screen was performed twice per cell line, and synergy scores were averaged. (B) Representative dose−response curves from the antagonistic combination of proteasome-Hsp90 inhibitors. In each example, the proteasome inhibitor (bortezomib) alone is shown in black, while the combinations with the Hsp90 inhibitor 17-DMAG are shown with blue lines. Results are the average of quadruplicate experiments and error bars are SD. Some error bars are smaller than the symbols. (C) Hsp72 is upregulated following Hsp90 and proteasome inhibition in all of the cell lines tested, by Western blot. Results are representative of experiments performed in triplicate. See the methods section for the concentrations used.

been shown to target mitochondrial Hsp70,[48,61] and it seems likely that, in these cells, it impacts mitochondrial proteostasis.

Immunoblotting Validates the RNA-Seq Results and Highlights Differences in Stress Responses Caused by Proteostasis Inhibition. To validate a subset of these RNA-seq findings, we examined the protein levels of representative stress response effectors, BiP (marker of the UPR) and Hsp72 (marker of the HSR), following proteostasis inhibition in the treated 22Rv1 cells (Figure 6C). We also monitored the levels of Hsc70/HSPA8, which is typically more mildly upregulated in the HSR. After 24 h of compound treatment, we observe BiP upregulation following inhibition of the proteasome or p97 and after treatment with the p97 inhibitor or the combinations of p97-proteasome or Hsp90-proteasome inhibitors, which is consistent with the RNA-seq results. In multiple myeloma cells, inhibitors of p97 have also been shown to activate the UPR, leading to elevated BiP levels.[22] Additionally, we observed that Hsp72 is elevated following treatment with either the Hsp90 inhibitor, the proteasome inhibitor, or the Hsp90-proteasome inhibitor combination in 22Rv1 cells (Figure 6C). Interestingly, the response to the combination was generally stronger than Hsp90 or proteasome inhibition alone, consistent with the RNA-seq results. Thus, we hypothesized that one mechanism driving antagonism between Hsp90 and proteasome inhibitors may be the strong upregulation of HSR genes, which might blunt the activity of

https://doi.org/10.1021/acs.jmedchem.1c01342
J. Med. Chem. 2021, 64, 14809−14821

both compounds. To test this idea, we combined proteasome inhibitor treatment with heat stress instead of the Hsp90 inhibitor. This experiment was designed to discern whether the antagonism was due to the effects of the Hsp90 inhibitor on the HSR or its ability to destabilize the chaperone's clients.[62,63] Accordingly, 22Rv1 cells were placed at 42 °C for either 15, 30, or 120 min and then treated with bortezomib. One important caveat in this experiment is that we were unable to maintain heat shock during the entire 72 h growth phase that is required for bortezomib-mediated antiproliferative activity. However, even with this caveat, it was still striking that the potency of bortezomib was unchanged by any of the heat shock treatments (Figure S4). Thus, the antagonism between inhibitors of Hsp90 and the proteasome might potentially involve destabilization of Hsp90 clients.

Additional Prostate Cancer Cell Lines Have both Similar and Distinct Patterns of Sensitivity to Proteostasis Inhibitors. Lastly, we probed how these patterns of drug synergy/antagonism might compare across other prostate cancer cell lines. For these studies, we chose three cell lines: LNCaP, C4-2, and PC-3. Briefly, LNCaP cells are an androgen-sensitive prostate cell line, and C4-2 cells are an androgen-insensitive cell line derived from LNCaP. Like 22Rv1 cells, both LNCaP and C4-2 express AR and are driven by AR signaling, while PC-3 cells are a prostate line that are androgen-insensitive and do not express AR. Thus, we expected that screens in these cell lines could reveal potential synergies across a wider range of prostate cancer cell types with different origins, AR status, and anti-androgen sensitivities.

We treated the three cell lines with an 8×8 matrix of compounds and summarized the resulting additivity, synergy, and antagonism through calculations of ZIP synergy scores. In Figure 7, we also include the results from the 22Rv1 cell lines (see Figure 3) again for clarity and comparison. Together, the results revealed that there are some similarities across the prostate cancer cell lines but that none of them respond exactly the same way (Figure 7A). Among the similarities, the combination of Hsp70-p97 inhibitors tended to be synergistic (ZIP values between +1.2 and 3.2) and the combination of Hsp90-proteasome inhibitors was always antagonistic (ZIP synergy values between −6.9 and −19.9). The shared antagonistic response to combinations of Hsp90 and proteasome inhibitors was especially intriguing. Examination of the dose−response curves from this series confirmed that the proteasome inhibitor (bortezomib) was toxic to all the cells but that addition of the Hsp90 inhibitor (17-DMAG) could make the compound less effective (Figure 7B), although this effect was more modest in the PC-3 cells. To explore whether this antagonism might be linked to upregulation of Hsp72, we performed Western blotting on the treated lysates. As we observed in the 22Rv1 cells, addition of an Hsp90 inhibitor to the proteasome inhibitor strongly upregulates Hsp72 at 24 h in each cell line (Figure 7C) and the level of elevation was greater than with either compound alone. There are hundreds of known Hsp90 clients;[62,63] so we have not yet been able to explore whether destabilization of these might be linked to antagonism across the four cell lines.

In addition to these similarities across the four cell lines, we also noted that some relationships depend on the cell type. For example, the combination of Hsp70-Hsp90 inhibitors was only synergistic (ZIP score, +2.4) in the 22Rv1 cells (Figure 7A) and was generally antagonistic in the other cell lines (ZIP scores between −4.4 and −4.9). 22Rv1 cells are the only line tested here that expresses both AR and ARv, so this could be one contributing factor (see Figure 3). Indeed, ARv has been shown to drive both overlapping and unique transcriptional programs, compared to AR;[64] thus, loss of both factors might be especially required in 22Rv1 cells. Together, these results highlight the importance of characterizing the wiring of the proteostasis network in each cell line or tumor model because the exact pattern of synergy/antagonism can depend on the cell type.

DISCUSSION

The proteostasis network holds great promise as a source of drug targets for anticancer treatment.[9,65] However, this concept has met with both successes and failures in the clinic, perhaps requiring a re-examination of the treatment strategies. One logical approach is to use inhibitor combinations, which might limit the ability of cancer proteostasis networks to compensate for the loss of one pathway. Although it had been hypothesized that combinations of proteostasis inhibitors might have additivity or even synergy in cancer cells, this possibility had not been systematically quantified. Using a high-throughput platform, we revealed clear and reproducible patterns of additivity, synergy, and antagonism between inhibitors of four major proteostasis nodes in four different prostate cancer cell lines. We observed that p97 and proteasome inhibitors were especially synergistic in 22Rv1 cells (ZIP score, 9.1), a model of castration-resistant prostate cancer (CRPC). Thus, this combination might be used to reduce the dose required for both compounds, potentially improving potency while reducing toxicity. In support of this idea, the p97-proteasome inhibitor combination did not produce enhanced cell growth inhibition in non-tumorigenic RWPE-1 cells (see Figure S2B). However, it is also important to note that synergy for this combination was not observed in the other three prostate cancer lines, where this combination was modestly antagonistic. Thus, a tailored therapeutic strategy might be required, such as screening primary cells against combinations *ex vivo* to identify synergistic relationships. Future work will be required to understand whether expression and stability of AR and ARv (see Figure 4A) are predictive of this synergy, as the 22Rv1 cells are the only line tested in this study that expresses both.

We were initially surprised to find drug combinations, exemplified by the Hsp90 and proteasome inhibitor pair, that showed striking antagonism. Within the chosen subnetwork (see Figure 1A), we initially hypothesized that synergy might predominate because of the collaboration between these factors. However, recent studies have introduced the idea of "single-agent dominance" in two-drug combinations.[66] In this paradigm, molecules that produce a faster onset of cell death can dominate the co-treatment because of cross talk between cell death pathways. Inhibition of Hsp70, for example, has been shown to rapidly induce both apoptosis and necroptosis,[67] so a deeper exploration of the role of cell death pathways and their kinetics will need to be explored for proteostasis inhibitors. Another possibility, potentially supported by our RNA-seq and Western blot findings and not mutually exclusive of "single-agent dominance", is that the stress responses might be partially responsible for the relationships between compound treatments. For example, the prostate cancer cells might activate the HSR to compensate for the loss of function of either Hsp90 or the proteasome. In support of this idea, the combination produces a more robust HSR activation (see

https://doi.org/10.1021/acs.jmedchem.1c01342
J. Med. Chem. 2021, 64, 14809−14821

Figure 7C). However, the combination of heat shock with the proteasome inhibitor was not antagonistic (see Figure S4), suggesting that other factors, such as destabilization of Hsp90 client proteins, might also play an important role. Hsp90 regulates the stability of hundreds of client proteins,[62,63] and it remains to be seen which ones might be involved in antagonism. Regardless, some evidence suggests that the relationship between Hsp90 and proteasome inhibitors might also depend on the type of cancers. For example, in multiple myeloma cells, treatment with a combination of Hsp90 and proteasome inhibitors has been suggested to be potentially synergistic based on preclinical studies,[68,69] and a clinical trial was conducted in multiple myeloma patients.[69,70] While our studies were done on prostate cancer cells, and not multiple myeloma, it seems possible that stratifying patients based on induction of the HSR and/or destabilization of Hsp90 clients might have helped parse the most likely to respond favorably.

Together, these results suggest that a more comprehensive understanding of which stress pathways are activated by proteostasis inhibitors is likely needed to better track and, ultimately, predict synergy/antagonism, with the goal of designing more effective treatment strategies. One major goal of those efforts could be to profile which stress response pathways, such as HSR, UPR, autophagy, etc., are activated by inhibitors so that predictive biomarkers could be identified.[71,72] Moreover, a deeper understanding of which Hsp90 clients are destabilized by inhibitors in specific cell types is lacking. Finally, it is starting to become clear that this framework could be more broadly important outside proteostasis targets as well. For example, treatment with other chemotherapeutics and radiation is capable of eliciting stress responses,[73,74] which might likewise blunt their efficacy. Thus, clinical biomarkers of stress responses might have important impacts outside programs associated with proteostasis targets.

EXPERIMENTAL SECTION

Cell Lines. 22Rv1, LNCaP, C4-2, and PC-3 cells were purchased from ATCC and grown in an RPMI 1640 medium supplemented with 10% non-heat-inactivated FBS (Gibco 16000044) and 1% penicillin/streptomycin. RWPE-1 cells were purchased from ATCC and grown in K-SFM supplemented with bovine pituitary extract and human recombinant EGF. All cells were grown at 37 °C and 5% CO_2. Cells were regularly tested for mycobacterial contamination (every 6 months) and maintained at a low passage number.

Inhibitors. JG-98 was prepared, as described,[48] and determined to be >95% pure by HPLC. 17-DMAG was purchased from Cayman Chemical (item #11036). CB-5083 was purchased from Fisher Scientific (catalog #50-115-2549). Bortezomib was purchased from Millipore Sigma (CAS 179324-69-7). AUY-922 was purchased from Fisher Scientific (CAS #747412-49-3). Commercial compounds are reported by the manufacturer to be 95% pure by HPLC.

Drug Combinations and Synergy. All tested compounds were prepared as 10 mM stocks in DMSO and stored in aliquots at −20 °C. For treatments, compounds were then serially diluted in twofold increments in RPMI (final DMSO, ∼0.02%). These solutions were then aliquoted to 96-well plates in an 8×8 matrix format for each combination. Concentrations were chosen based on the EC_{50} value of each compound in the cell lines tested, to center the dilution series on the half-maximal value. Specifically, the following final concentrations were used: JG-98 (0.16 to 10 μM), 17-DMAG (0.016 to 1 μM), CB-5083 (0.078 to 5 μM), bortezomib (0.0015 to 0.1 μM). Each compound was tested in 7 doses (plus a DMSO solvent control), using twofold serial dilutions.

Cells were grown in tissue-culture-treated 384-well plates (Corning). After 24 h of cell growth, an Agilent robot was used to transfer compounds from the 96-well plates to these 384-well test plates. Cells were returned to 37 °C and 5% CO_2 and grown for 3 days (doubling time 30−50 h depending on the cell line). Cell viability was measured using Cell Titer Glo (Promega) according to the manufacturer's instructions, and luminescence was measured using a SpectraMax M5 plate reader (Molecular Devices). Cell viability was normalized per plate to the untreated, DMSO control. Synergy was determined using SynergyFinger (http://www.synergyfinderplus.org/). All drug combinations were performed twice per cell line (in technical quadruplicates), and the average mean synergy score for the entire dataset was reported.

Immunoblotting. Cells were plated in 6-well or 12-well plates at 80−100% confluency for 24 h, after which the medium was replaced with a fresh medium containing indicated compounds at 1% DMSO. Compounds were left on cells for the indicated time period (6−24 h), and cells were incubated at 37 °C and 5% CO_2. Cell lysate was then harvested with M-PER supplemented with the protease inhibitor. For measuring phospho-proteins, M-PER was additionally supplemented with a phosphatase inhibitor. Lysate was then run on 4−15% gradient SDS polyacrylamide gels at 5−10 μg of total protein per sample. Protein levels were detected either with Licor fluorescent secondary antibodies and detected with a Licor machine or with HRP-conjugated secondary antibodies and imaged with BioRad. The following antibodies were used.

Antibodies. The following antibodies were used for immunoblotting: AR (Abcam #ab133273, 1:2000, rabbit), BiP (CST #3177, 1:2000, rabbit), Hsc70/HSPA8 (Enzo ADI-SPA-816-F, 1:2000, rabbit), Hsp72/HSPA1A (Enzo ADI-SPA-811-F, 1:2000, rabbit), and actin (Sigma A2228, 1:5000, mouse).

RNA-Seq and Western Blot Validation. Treatment concentrations were chosen based on dose−response and drug synergy data, to best capture combinations of compounds that were either synergistic or antagonistic. Specifically, the following concentrations were used: JG-98 (0.625 μM), 17-DMAG (0.25 μM), CB-5083 (0.625 μM), and bortezomib (0.025 μM).

For RNA-seq studies, 22Rv1 cells were plated at 80% confluency in 12-well plates. After 24 h, cells were dosed with compounds at indicated concentrations and incubated at 37 °C and 5% CO_2. After 6 h treatment, RNA was extracted using a Zymo Quick-RNA miniprep kit (Catalog #R1054). RNAs from all samples were diluted to 20 ng/μL in 10 μL for input into TECAN Universal plus mRNA-seq library preparation. RNA-Seq libraries were prepared using the manufacture's protocol. RNA-Seq libraries were sequenced for quality control on an Illumina MiniSeq and pooled according to protein coding read counts to obtain uniform protein coding read depth. The final pools were sequenced using single-end 50 bp reads on an Illumina HiSeq 4000 at the Center for Advanced Technology (www.cat.ucsf.edu). Sequencing reads were aligned to the Human reference genome (Build HG38) and the Ensembl gene annotation (version 95) using STAR (v2.7.2b; PMID: 23104886). Read counts per gene as output by STAR were collapsed into a read counts matrix and were used as input to DESeq2 (v1.24.0; PMID: 25516281) to test for differential gene expression between conditions using a Wald test. Genes passing a multiple testing correct p-value of 0.1 (FDR method) were considered significant. For Western blot validation of RNA-seq, 22Rv1 cells were plated and dosed under the same conditions. Following drug-treatment, immunoblotting was performed as described above.

ASSOCIATED CONTENT

Supporting Information

The Supporting Information is available free of charge at https://pubs.acs.org/doi/10.1021/acs.jmedchem.1c01342.

(Figures S1−S4) Evidence of reproducibility in 22Rv1 cells treated with proteostasis inhibitor combinations, control studies performed with the proteostasis inhibitors, effects of additional proteostasis inhibitor combinations on AR levels in 22Rv1 cells, and heat shock (HS) does not affect bortezomib potency in 22Rv1 cells (PDF)

https://doi.org/10.1021/acs.jmedchem.1c01342
J. Med. Chem. 2021, 64, 14809−14821

AUTHOR INFORMATION

Corresponding Author

Jason E. Gestwicki − *Department of Pharmaceutical Chemistry and Institute for Neurodegenerative Disease, University of California San Francisco, San Francisco, California 94158, United States;* orcid.org/0000-0002-6125-3154; Phone: 415-502-7121; Email: jason.gestwicki@ucsf.edu

Authors

Arielle Shkedi − *Department of Pharmaceutical Chemistry and Institute for Neurodegenerative Disease, University of California San Francisco, San Francisco, California 94158, United States*

Michael Adkisson − *Functional Genomics Core, University of California San Francisco, San Francisco, California 94158, United States*

Andrew Schroeder − *Functional Genomics Core, University of California San Francisco, San Francisco, California 94158, United States*

Walter L Eckalbar − *Functional Genomics Core, University of California San Francisco, San Francisco, California 94158, United States*

Szu-Yu Kuo − *Department of Pharmaceutical Chemistry and Institute for Neurodegenerative Disease, University of California San Francisco, San Francisco, California 94158, United States*

Leonard Neckers − *Urologic Oncology Branch, Center for Cancer Research, National Cancer Institute, Bethesda, Maryland 20892, United States*

Complete contact information is available at: https://pubs.acs.org/10.1021/acs.jmedchem.1c01342

Notes

The authors declare the following competing financial interest(s): J.E.G. is an inventor on patents associated with Hsp70 inhibitors and their use in cancer.

ACKNOWLEDGMENTS

This work was supported by grants from the US Department of Defense (PC180716 and PC150065; to J.E.G. and L.N.), the NIH (NS059690 to J.E.G.), and the Mary A. Koda-Kimble Seed Award (to A.S.). The authors additionally thank S. Sannino and J. Brodsky (U. Pittsburgh) and A. Witta (UCSF) for helpful comments and advice.

ABBREVIATIONS USED

AR, androgen receptor; ARv, androgen receptor variant; 17-DMAG, 17-dimethylaminoethylamino-17-demethoxygeldanamycin; ERAD, Endoplasic reticulum-associated degradation; ISR, integrated stress response; Hop, Hsp70-organizing protein; HSF1, heat shock factor 1; Hsp70, heat shock protein 70; Hsp90, heat shock protein 90; HSR, heat shock response; UPR, unfolded protein response; VCP, valosin-containing protein

REFERENCES

(1) Powers, E. T.; Morimoto, R. I.; Dillin, A.; Kelly, J. W.; Balch, W. E. Biological and chemical approaches to diseases of proteostasis deficiency. *Annu. Rev. Biochem.* **2009**, *78*, 959−991.

(2) Voisine, C.; Pedersen, J. S.; Morimoto, R. I. Chaperone networks: Tipping the balance in protein folding diseases. *Neurobiol Dis* **2010**, *40*, 12−20.

(3) Labbadia, J.; Morimoto, R. I. The biology of proteostasis in aging and disease. *Annu. Rev. Biochem.* **2015**, *84*, 435−464.

(4) Freilich, R.; Arhar, T.; Abrams, J. L.; Gestwicki, J. E. Protein-protein interactions in the molecular chaperone network. *Acc. Chem. Res.* **2018**, *51*, 940−949.

(5) Liu, Y.; Ye, Y. Proteostasis regulation at the endoplasmic reticulum: A new perturbation site for targeted cancer therapy. *Cell Research* **2011**, *21*, 867−883.

(6) Whitesell, L.; Bagatell, R.; Falsey, R. The stress response: Implications for the clinical development of hsp90 inhibitors. *Curr. Cancer Drug Targets* **2003**, *3*, 349−358.

(7) Dai, C.; Whitesell, L.; Rogers, A. B.; Lindquist, S. Heat shock factor 1 is a powerful multifaceted modifier of carcinogenesis. *Cell* **2007**, *130*, 1005−1018.

(8) Pakos-Zebrucka, K.; Koryga, I.; Mnich, K.; Ljujic, M.; Samali, A.; Gorman, A. M. The integrated stress response. *EMBO Rep.* **2016**, *17*, 1374−1395.

(9) Joshi, S.; Wang, T.; Araujo, T. L. S.; Sharma, S.; Brodsky, J. L.; Chiosis, G. Adapting to stress - chaperome networks in cancer. *Nature reviews* **2018**, *18*, 562−575.

(10) Workman, P.; Burrows, F.; Neckers, L.; Rosen, N. Drugging the cancer chaperone hsp90: Combinatorial therapeutic exploitation of oncogene addiction and tumor stress. *Ann. N. Y. Acad. Sci.* **2007**, *1113*, 202−216.

(11) Calderwood, S. K.; Gong, J. Heat shock proteins promote cancer: It's a protection racket. *Trends Biochem. Sci.* **2016**, *41*, 311−323.

(12) Whitesell, L.; Lindquist, S. Inhibiting the transcription factor hsf1 as an anticancer strategy. *Expert Opin Ther Targets* **2009**, *13*, 469−478.

(13) Gabai, V. L.; Yaglom, J. A.; Wang, Y.; Meng, L.; Shao, H.; Kim, G.; Colvin, T.; Gestwicki, J.; Sherman, M. Y. Anticancer effects of targeting hsp70 in tumor stromal cells. *Cancer Res.* **2016**, *76*, 5926−5932.

(14) Hadizadeh Esfahani, A.; Sverchkova, A.; Saez-Rodriguez, J.; Schuppert, A. A.; Brehme, M. A systematic atlas of chaperome deregulation topologies across the human cancer landscape. *PLoS Comput. Biol.* **2018**, *14*, No. e1005890.

(15) Rodina, A.; Wang, T.; Yan, P.; Gomes, E. D.; Dunphy, M. P.; Pillarsetty, N.; Koren, J.; Gerecitano, J. F.; Taldone, T.; Zong, H.; Caldas-Lopes, E.; Alpaugh, M.; Corben, A.; Riolo, M.; Beattie, B.; Pressl, C.; Peter, R. I.; Xu, C.; Trondl, R.; Patel, H. J.; Shimizu, F.; Bolaender, A.; Yang, C.; Panchal, P.; Farooq, M. F.; Kishinevsky, S.; Modi, S.; Lin, O.; Chu, F.; Patil, S.; Erdjument-Bromage, H.; Zanzonico, P.; Hudis, C.; Studer, L.; Roboz, G. J.; Cesarman, E.; Cerchietti, L.; Levine, R.; Melnick, A.; Larson, S. M.; Lewis, J. S.; Guzman, M. L.; Chiosis, G. The epichaperome is an integrated chaperome network that facilitates tumour survival. *Nature* **2016**, *538*, 397−401.

(16) Evans, C. G.; Chang, L.; Gestwicki, J. E. Heat shock protein 70 (hsp70) as an emerging drug target. *J. Med. Chem.* **2010**, *53*, 4585−4602.

(17) Urra, H.; Dufey, E.; Avril, T.; Chevet, E.; Hetz, C. Endoplasmic reticulum stress and the hallmarks of cancer. *Trends Cancer* **2016**, *2*, 252−262.

(18) Ruan, L.; Wang, Y.; Zhang, X.; Tomaszewski, A.; McNamara, J. T.; Li, R. Mitochondria-associated proteostasis. *Annu. Rev. Biophys.* **2020**, *49*, 41−67.

(19) Workman, P.; Powers, M. V. Chaperoning cell death: A critical dual role for hsp90 in small-cell lung cancer. *Nat. Chem. Biol.* **2007**, *3*, 455−457.

(20) Dong, B.; Jaeger, A. M.; Hughes, P. F.; Loiselle, D. R.; Hauck, J. S.; Fu, Y.; Haystead, T. A.; Huang, J.; Thiele, D. J. Targeting therapy-resistant prostate cancer via a direct inhibitor of the human heat shock transcription factor 1. *Science Trans. Med.* **2020**, *12*, eabb5647.

(21) Mishra, S.; Liu, W.; Beebe, K.; Banerjee, M.; Kent, C. N.; Munthali, V.; Koren, J., 3rd; Taylor, J. A., 3rd; Neckers, L. M.; Holzbeierlein, J.; Blagg, B. S. J. The development of hsp90beta-

selective inhibitors to overcome detriments associated with pan-hsp90 inhibition. *J. Med. Chem.* **2021**, *64*, 1545−1557.
(22) Anderson, D. J.; Le Moigne, R.; Djakovic, S.; Kumar, B.; Rice, J.; Wong, S.; Wang, J.; Yao, B.; Valle, E.; Kiss von Soly, S.; Madriaga, A.; Soriano, F.; Menon, M. K.; Wu, Z. Y.; Kampmann, M.; Chen, Y.; Weissman, J. S.; Aftab, B. T.; Yakes, F. M.; Shawver, L.; Zhou, H. J.; Wustrow, D.; Rolfe, M. Targeting the aaa atpase p97 as an approach to treat cancer through disruption of protein homeostasis. *Cancer Cell* **2015**, *28*, 653−665.
(23) Manasanch, E. E.; Orlowski, R. Z. Proteasome inhibitors in cancer therapy. *Nat Rev Clin Oncol* **2017**, *14*, 417−433.
(24) Garg, G.; Khandelwal, A.; Blagg, B. S. J. Anticancer inhibitors of hsp90 function: Beyond the usual suspects. *Adv Cancer Res* **2016**, *129*, 51−88.
(25) Chatterjee, S.; Bhattacharya, S.; Socinski, M. A.; Burns, T. F. Hsp90 inhibitors in lung cancer: Promise still unfulfilled. *Clin Adv Hematol Oncol* **2016**, *14*, 346−356.
(26) Goloudina, A. R.; Demidov, O. N.; Garrido, C. Inhibition of hsp70: A challenging anti-cancer strategy. *Cancer Lett.* **2012**, *325*, 117−124.
(27) Huang, Z.; Wu, Y.; Zhou, X.; Xu, J.; Zhu, W.; Shu, Y.; Liu, P. Efficacy of therapy with bortezomib in solid tumors: A review based on 32 clinical trials. *Future Oncology* **2014**, *10*, 1795−1807.
(28) Sannino, S.; Guerriero, C. J.; Sabnis, A. J.; Stolz, D. B.; Wallace, C. T.; Wipf, P.; Watkins, S. C.; Bivona, T. G.; Brodsky, J. L. Compensatory increases of select proteostasis networks after hsp70 inhibition in cancer cells. *J. Cell Sci.* **2018**, *131*, PMC6140321.
(29) Zhu, K.; Dunner, K., Jr.; McConkey, D. J. Proteasome inhibitors activate autophagy as a cytoprotective response in human prostate cancer cells. *Oncogene* **2010**, *29*, 451−462.
(30) Sannino, S.; Yates, M. E.; Schurdak, M. E.; Oesterreich, S.; Lee, A. V.; Wipf, P.; Brodsky, J. L. Unique integrated stress response sensors regulate cancer cell susceptibility when hsp70 activity is compromised. *eLife* **2021**, *10*, No. e64977.
(31) Shah, S. P.; Nooka, A. K.; Jaye, D. L.; Bahlis, N. J.; Lonial, S.; Boise, L. H. Bortezomib-induced heat shock response protects multiple myeloma cells and is activated by heat shock factor 1 serine 326 phosphorylation. *Oncotarget* **2016**, *7*, 59727−59741.
(32) Bai, Y.; Su, X. Updates to the drug-resistant mechanism of proteasome inhibitors in multiple myeloma. *Asia Pac J Clin Oncol* **2021**, *17*, 29−35.
(33) Powers, M. V.; Clarke, P. A.; Workman, P. Dual targeting of hsc70 and hsp72 inhibits hsp90 function and induces tumor-specific apoptosis. *Cancer Cell* **2008**, *14*, 250−262.
(34) Shevtsov, M.; Multhoff, G.; Mikhaylova, E.; Shibata, A.; Guzhova, I.; Margulis, B. Combination of anti-cancer drugs with molecular chaperone inhibitors. *Int. J. Mol. Sci.* **2019**, *20*, 5284.
(35) Eugenio, A. I. P.; Fook-Alves, V. L.; de Oliveira, M. B.; Fernando, R. C.; Zanatta, D. B.; Strauss, B. E.; Silva, M. R. R.; Porcionatto, M. A.; Colleoni, G. W. B. Proteasome and heat shock protein 70 (hsp70) inhibitors as therapeutic alternative in multiple myeloma. *Oncotarget* **2017**, *8*, 114698−114709.
(36) Cavanaugh, A.; Juengst, B.; Sheridan, K.; Danella, J. F.; Williams, H. Combined inhibition of heat shock proteins 90 and 70 leads to simultaneous degradation of the oncogenic signaling proteins involved in muscle invasive bladder cancer. *Oncotarget* **2015**, *6*, 39821−39838.
(37) Moses, M. A.; Kim, Y. S.; Rivera-Marquez, G. M.; Oshima, N.; Watson, M. J.; Beebe, K.; Wells, C.; Lee, S.; Zuehlke, A. D.; Shao, H.; Bingman, W. E.; Kumar, V.; Malhotra, S.; Weigel, N. L.; Gestwicki, J. E.; Trepel, J.; Neckers, L. M. Targeting the hsp40/hsp70 chaperone axis as a novel strategy to treat castration-resistant prostate cancer. *Cancer Res.* **2018**, *78*, 4022−4035.
(38) Echeverria, P. C.; Picard, D. Molecular chaperones, essential partners of steroid hormone receptors for activity and mobility. *Biochim. Biophys. Acta* **2010**, *1803*, 641−649.
(39) Hartl, F. U.; Hayer-Hartl, M. Converging concepts of protein folding in vitro and in vivo. *Nat. Struct. Mol. Biol.* **2009**, *16*, 574−581.
(40) Vekaria, P. H.; Home, T.; Weir, S.; Schoenen, F. J.; Rao, R. Targeting p97 to disrupt protein homeostasis in cancer. *Front. Oncol.* **2016**, *6*, 181.
(41) Collins, G. A.; Goldberg, A. L. The logic of the 26s proteasome. *Cell* **2017**, *169*, 792−806.
(42) Johnson, B. D.; Schumacher, R. J.; Ross, E. D.; Toft, D. O. Hop modulates hsp70/hsp90 interactions in protein folding. *J Biol Chem* **1998**, *273*, 3679−3686.
(43) Kirschke, E.; Goswami, D.; Southworth, D.; Griffin, P. R.; Agard, D. A. Glucocorticoid receptor function regulated by coordinated action of the hsp90 and hsp70 chaperone cycles. *Cell* **2014**, *157*, 1685−1697.
(44) Lemberg, M. K.; Strisovsky, K. Maintenance of organellar protein homeostasis by er-associated degradation and related mechanisms. *Mol. Cell* **2021**, *81*, 2507−2519.
(45) Brodsky, J. L. The protective and destructive roles played by molecular chaperones during erad (endoplasmic-reticulum-associated degradation). *Biochem. J.* **2007**, *404*, 353−363.
(46) Petrucelli, L.; Dickson, D.; Kehoe, K.; Taylor, J.; Snyder, H.; Grover, A.; De Lucia, M.; McGowan, E.; Lewis, J.; Prihar, G.; Kim, J.; Dillmann, W. H.; Browne, S. E.; Hall, A.; Voellmy, R.; Tsuboi, Y.; Dawson, T. M.; Wolozin, B.; Hardy, J.; Hutton, M. Chip and hsp70 regulate tau ubiquitination, degradation and aggregation. *Hum. Mol. Genet.* **2004**, *13*, 703−714.
(47) Dickey, C. A.; Kamal, A.; Lundgren, K.; Klosak, N.; Bailey, R. M.; Dunmore, J.; Ash, P.; Shoraka, S.; Zlatkovic, J.; Eckman, C. B.; Patterson, C.; Dickson, D. W.; Nahman, N. S., Jr.; Hutton, M.; Burrows, F.; Petrucelli, L. The high-affinity hsp90-chip complex recognizes and selectively degrades phosphorylated tau client proteins. *J Clin Invest* **2007**, *117*, 648−658.
(48) Li, X.; Srinivasan, S. R.; Connarn, J.; Ahmad, A.; Young, Z. T.; Kabza, A. M.; Zuiderweg, E. R.; Sun, D.; Gestwicki, J. E. Analogs of the allosteric heat shock protein 70 (hsp70) inhibitor, mkt-077, as anti-cancer agents. *ACS Med. Chem. Lett.* **2013**, *4*, 1042−1047.
(49) Goetz, M. P.; Toft, D. O.; Ames, M. M.; Erlichman, C. The hsp90 chaperone complex as a novel target for cancer therapy. *Ann. Oncol.* **2003**, *14*, 1169−1176.
(50) Arkwright, R.; Pham, T. M.; Zonder, J. A.; Dou, Q. P. The preclinical discovery and development of bortezomib for the treatment of mantle cell lymphoma. *Expert Opin. Drug Discovery* **2017**, *12*, 225−235.
(51) Kaul, S. C.; Deocaris, C. C.; Wadhwa, R. Three faces of mortalin: A housekeeper, guardian and killer. *Exp Gerontol* **2007**, *42*, 263−274.
(52) Yadav, B.; Wennerberg, K.; Aittokallio, T.; Tang, J. Searching for drug synergy in complex dose-response landscapes using an interaction potency model. *Comput Struct Biotechnol J* **2015**, *13*, 504−513.
(53) Tallarida, R. J. Quantitative methods for assessing drug synergism. *Genes Cancer* **2011**, *2*, 1003−1008.
(54) Chou, T. C.; Talalay, P. Quantitative analysis of dose-effect relationships: The combined effects of multiple drugs or enzyme inhibitors. *Adv. Enzyme Regul.* **1984**, *22*, 27−55.
(55) Meyer, C. T.; Wooten, D. J.; Lopez, C. F.; Quaranta, V. Charting the fragmented landscape of drug synergy. *Trends Pharm Sci* **2020**, *41*, 266−280.
(56) Vlot, A. H. C.; Aniceto, N.; Menden, M. P.; Ulrich-Merzenich, G.; Bender, A. Applying synergy metrics to combination screening data: Agreements, disagreements and pitfalls. *Drug Discovery Today* **2019**, *24*, 2286−2298.
(57) Feng, Q.; He, B. Androgen receptor signaling in the development of castration-resistant prostate cancer. *Front. Oncol.* **2019**, *9*, 858.
(58) Watson, P. A.; Arora, V. K.; Sawyers, C. L. Emerging mechanisms of resistance to androgen receptor inhibitors in prostate cancer. *Nat. Rev. Cancer* **2015**, *15*, 701−711.
(59) Eftekharzadeh, B.; Banduseela, V. C.; Chiesa, G.; Martinez-Cristobal, P.; Rauch, J. N.; Nath, S. R.; Schwarz, D. M. C.; Shao, H.; Marin-Argany, M.; Di Sanza, C.; Giorgetti, E.; Yu, Z.; Pierattelli, R.;

https://doi.org/10.1021/acs.jmedchem.1c01342
J. Med. Chem. 2021, 64, 14809−14821

Felli, I. C.; Brun-Heath, I.; Garcia, J.; Nebreda, A. R.; Gestwicki, J. E.; Lieberman, A. P.; Salvatella, X. Hsp70 and hsp40 inhibit an inter-domain interaction necessary for transcriptional activity in the androgen receptor. *Nat. Commun.* **2019**, *10*, 3562.
(60) Anckar, J.; Sistonen, L. Regulation of hsf1 function in the heat stress response: Implications in aging and disease. *Annu. Rev. Biochem.* **2011**, *80*, 1089−1115.
(61) Wadhwa, R.; Sugihara, T.; Yoshida, A.; Nomura, H.; Reddel, R. R.; Simpson, R.; Maruta, H.; Kaul, S. C. Selective toxicity of mkt-077 to cancer cells is mediated by its binding to the hsp70 family protein mot-2 and reactivation of p53 function. *Cancer Res.* **2000**, *60*, 6818−6821.
(62) Taipale, M.; Tucker, G.; Peng, J.; Krykbaeva, I.; Lin, Z. Y.; Larsen, B.; Choi, H.; Berger, B.; Gingras, A. C.; Lindquist, S. A quantitative chaperone interaction network reveals the architecture of cellular protein homeostasis pathways. *Cell* **2014**, *158*, 434−448.
(63) Whitesell, L.; Mimnaugh, E. G.; De Costa, B.; Myers, C. E.; Neckers, L. M. Inhibition of heat shock protein hsp90-pp60v-src heteroprotein complex formation by benzoquinone ansamycins: Essential role for stress proteins in oncogenic transformation. *Proc. Natl. Acad. Sci. U. S. A.* **1994**, *91*, 8324−8328.
(64) Hu, R.; Lu, C.; Mostaghel, E. A.; Yegnasubramanian, S.; Gurel, M.; Tannahill, C.; Edwards, J.; Isaacs, W. B.; Nelson, P. S.; Bluemn, E.; Plymate, S. R.; Luo, J. Distinct transcriptional programs mediated by the ligand-dependent full-length androgen receptor and its splice variants in castration-resistant prostate cancer. *Cancer Res.* **2012**, *72*, 3457−3462.
(65) Sannino, S.; Brodsky, J. L. Targeting protein quality control pathways in breast cancer. *BMC Biol* **2017**, *15*, 109.
(66) Richards, R.; Schwartz, H. R.; Honeywell, M. E.; Stewart, M. S.; Cruz-Gordillo, P.; Joyce, A. J.; Landry, B. D.; Lee, M. J. Drug antagonism and single-agent dominance result from differences in death kinetics. *Nat. Chem. Biol.* **2020**, *16*, 791−800.
(67) Srinivasan, S. R.; Cesa, L. C.; Li, X.; Julien, O.; Zhuang, M.; Shao, H.; Chung, J.; Maillard, I.; Wells, J. A.; Duckett, C. S.; Gestwicki, J. E. Heat shock protein 70 (hsp70) suppresses rip1-dependent apoptotic and necroptotic cascades. *Molecular Cancer Res: MCR* **2018**, *16*, 58−68.
(68) Ishii, T.; Seike, T.; Nakashima, T.; Juliger, S.; Maharaj, L.; Soga, S.; Akinaga, S.; Cavenagh, J.; Joel, S.; Shiotsu, Y. Anti-tumor activity against multiple myeloma by combination of kw-2478, an hsp90 inhibitor, with bortezomib. *Blood Cancer J* **2012**, *2*, No. e68.
(69) Richardson, P. G.; Mitsiades, C. S.; Laubach, J. P.; Lonial, S.; Chanan-Khan, A. A.; Anderson, K. C. Inhibition of heat shock protein 90 (hsp90) as a therapeutic strategy for the treatment of myeloma and other cancers. *Br. J. Haematol.* **2011**, *152*, 367−379.
(70) Cavenagh, J.; Oakervee, H.; Baetiong-Caguioa, P.; Davies, F.; Gharibo, M.; Rabin, N.; Kurman, M.; Novak, B.; Shiraishi, N.; Nakashima, D.; Akinaga, S.; Yong, K. A phase i/ii study of kw-2478, an hsp90 inhibitor, in combination with bortezomib in patients with relapsed/refractory multiple myeloma. *Br. J. Cancer* **2017**, *117*, 1295−1302.
(71) Dhama, K.; Latheef, S. K.; Dadar, M.; Samad, H. A.; Munjal, A.; Khandia, R.; Karthik, K.; Tiwari, R.; Yatoo, M. I.; Bhatt, P.; Chakraborty, S.; Singh, K. P.; Iqbal, H. M. N.; Chaicumpa, W.; Joshi, S. K. Biomarkers in stress related diseases/disorders: Diagnostic, prognostic, and therapeutic values. *Frontiers Molec Biosci* **2019**, *6*, 91.
(72) Bagatell, R.; Paine-Murrieta, G. D.; Taylor, C. W.; Pulcini, E. J.; Akinaga, S.; Benjamin, I. J.; Whitesell, L. Induction of a heat shock factor 1-dependent stress response alters the cytotoxic activity of hsp90-binding agents. *Clin Cancer Res* **2000**, *6*, 3312−3318.
(73) Tiligada, E. Chemotherapy: Induction of stress responses. *Endocr.-Relat. Cancer* **2006**, *13*, S115−S124.
(74) Kim, W.; Lee, S.; Seo, D.; Kim, D.; Kim, K.; Kim, E.; Kang, J.; Seong, K. M.; Youn, H.; Youn, B. Cellular stress responses in radiotherapy. *Cell* **2019**, *8*, 1105.

https://doi.org/10.1021/acs.jmedchem.1c01342
J. Med. Chem. 2021, 64, 14809−14821

Article

Cell Chemical Biology

Selective vulnerabilities in the proteostasis network of castration-resistant prostate cancer

Graphical abstract

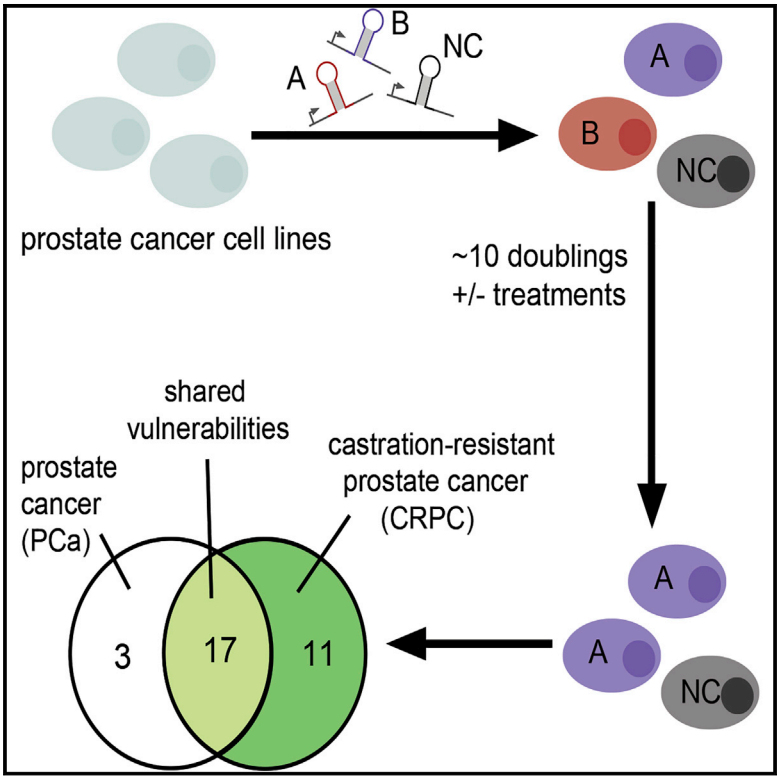

Highlights

- Prostate cancer cells depend on proteostasis pathways for survival
- Functional genomics screens revealed that CRPC cells depend on HSP60
- HSP60 is required for a CRPC-related metabolic switch, not AR stability
- HSP60 is a promising drug target for CRPC

Authors

Arielle Shkedi, Isabelle R. Taylor, Frank Echtenkamp, ..., Felix Feng, Martin Kampmann, Jason E. Gestwicki

Correspondence

jason.gestwicki@ucsf.edu

In brief

Drug targets for castration-resistant prostate cancer (CRPC) are needed. The protein homeostasis (proteostasis) pathways are known to include targets; however, a systematic search had not been performed. Here, Shkedi and Taylor et al. use an shRNA screen targeting ~130 proteostasis factors to identify HSP60 as a selective vulnerability in CRPC.

Shkedi et al., 2022, Cell Chemical Biology *29*, 490–501
March 17, 2022
https://doi.org/10.1016/j.chembiol.2022.01.008

CellPress

CellPress

Cell Chemical Biology

Article

Selective vulnerabilities in the proteostasis network of castration-resistant prostate cancer

Arielle Shkedi,[1,6] Isabelle R. Taylor,[1,6] Frank Echtenkamp,[3] Poornima Ramkumar,[2] Mohamed Alshalalfa,[4] Génesis M. Rivera-Márquez,[3] Michael A. Moses,[3] Hao Shao,[1] Robert Jeffrey Karnes,[5] Len Neckers,[3] Felix Feng,[4] Martin Kampmann,[2] and Jason E. Gestwicki[1,7,*]

[1]Department of Pharmaceutical Chemistry and the Institute for Neurodegenerative Disease, University of California, San Francisco, San Francisco, CA 94158, USA

[2]Department of Biochemistry and Biophysics and the Institute for Neurodegenerative Disease, University of California, San Francisco, San Francisco, CA 94158, USA

[3]Urologic Oncology Branch, Center for Cancer Research, National Cancer Institute, Bethesda, MD 20892, USA

[4]Radiation Oncology, Helen Diller Comprehensive Cancer Center, University of California, San Francisco, San Francisco, CA, USA

[5]Department of Urology, Mayo Clinic, Rochester, MN 55902, USA

[6]These authors contributed equally

[7]Lead contact

*Correspondence: jason.gestwicki@ucsf.edu

https://doi.org/10.1016/j.chembiol.2022.01.008

SUMMARY

Castration-resistant prostate cancer (CRPC) is associated with an increased reliance on heat shock protein 70 (HSP70), but it is not clear what other protein homeostasis (proteostasis) factors might be involved. To address this question, we performed functional and synthetic lethal screens in four prostate cancer cell lines. These screens confirmed key roles for HSP70, HSP90, and their co-chaperones, but also suggested that the mitochondrial chaperone, HSP60/HSPD1, is selectively required in CRPC cell lines. Knockdown of HSP60 does not impact the stability of androgen receptor (AR) or its variants; rather, it is associated with loss of mitochondrial spare respiratory capacity, partly owing to increased proton leakage. Finally, transcriptional data revealed a correlation between HSP60 levels and poor survival of prostate cancer patients. These findings suggest that re-wiring of the proteostasis network is associated with CRPC, creating selective vulnerabilities that might be targeted to treat the disease.

INTRODUCTION

Protein homeostasis (proteostasis) is achieved when the overall rates of protein folding, trafficking, and degradation are balanced (Balch et al., 2008). This balance is maintained by the proteostasis network, a collection of interconnected pathways that include molecular chaperones, stress response signaling factors, and protein quality control systems. In cancer cells, unique demands are placed on the proteostasis network, owing to their rapid growth rates, unusual metabolic requirements, and high mutational loads (Brodsky and Chiosis, 2006; Chaudhury et al., 2006; Powers et al., 2009; Whitesell and Lindquist, 2005). This dependence has been described as a "non-oncogene addiction" (Luo et al., 2009; Nagel et al., 2016), and individual components of the proteostasis network have been pursued as attractive anti-cancer targets. In the clinic, such attempts have yielded both dramatic successes and confounding failures (Crawford et al., 2011). One potential reason for this uneven level of success is that the field is only beginning to probe how proteostasis networks are functionally different in cancer cells versus normal cells or between different stages of cancer (Calderwood and Gong, 2016; Gabai et al., 2016; Rodina et al., 2016; Wu et al., 2020).

Prostate cancer (PCa) is an especially interesting system for probing these questions. PCa cells typically rely on transcriptional programs driven by the androgen receptor (AR), and many prostate tumors therefore initially respond well to androgen deprivation therapy (ADT). However, following ADT, the disease invariably progress to castration-resistant prostate cancer (CRPC) (Heinlein and Chang, 2004; Kirby et al., 2011; Logothetis et al., 2013). In CRPC cells, AR activity is usually able to persist through amplification, mutations, constitutively active splice variants of AR (ARv) (Antonarakis et al., 2014; Grasso et al., 2012; Montgomery et al., 2008; Quigley et al., 2018; Watson et al., 2015), and compensation by other steroid hormone receptors (SHRs), such as the glucocorticoid receptor (Arora et al., 2013; Puhr et al., 2018). Additionally, the conversion from PCa to CRPC is associated with metabolic reprogramming (Massie et al., 2011). Thus, it seems likely that to account for these molecular and metabolic changes, the proteostasis networks of PCa and CRPC cells might need to be

distinct. For example, similar to other SHRs, AR is known to require an elaborate set of chaperones, including heat shock protein 70 (HSP70), heat shock protein 90 (HSP90), and their co-chaperones, for its folding, activation, and degradation (Echeverria and Picard, 2010; Kirschke et al., 2014; Pratt et al., 2006; Pratt and Toft, 2003). Accordingly, chemical inhibitors of HSP90 are known to promote degradation of AR in PCa cells (Moses et al., 2018), and these inhibitors show synergy with ADT (Chen et al., 2016). Similar findings have been observed when targeting essential HSP90 co-chaperones (De Leon et al., 2011). However, HSP90 inhibitors are less effective in cellular models of CRPC, such as 22Rv1, which are partly driven by ARv signaling. Instead, inhibitors of HSP70 have been shown to decrease the stability of ARvs and have anti-proliferative activity in these cells (Moses et al., 2018). This difference in chaperone inhibitor sensitivity between PCa and CRPC cells might be partially explained by differences in molecular recognition of AR and its variants. Specifically, HSP70, but not HSP90, binds to the N-terminal motif that remains in the ARv found in 22Rv1 cells (Dong et al., 2019; Eftekharzadeh et al., 2019). Thus, CRPC is an interesting model for studying the role of proteostasis networks, given the reliance of these cells on HSP70, HSP90, and AR and its variants.

While there is growing evidence for the roles of HSP70 and HSP90 in PCa and CRPC, it is not yet clear whether the broader proteostasis network might be "re-wired" to accommodate the demands of CRPC. Here, we used functional genomics screening to identify selective vulnerabilities in PCa and CRPC cell lines. In that effort, we deployed a focused short hairpin RNA (shRNA) collection, termed the Proteostasis Library (Abrams et al., 2021), that allows knockdown of ~140 molecular chaperones, co-chaperones, chaperonins, and related factors. In addition, we searched for synthetic lethality by repeating the screens in the presence of chemical inhibitors of HSP70 and HSP90. Together, the results identified not only factors that are required in all the cells (e.g., shared vulnerabilities), but also factors that are unique to PCa or CRPC cell lines. One of the most striking findings was that the mitochondrial chaperonin, HSP60 (gene name HSPD1) is required for growth of CRPC cells, but not PCa cells. Knockdown studies suggest that, in contrast to HSP70 and HSP90, this chaperonin is not involved in AR or ARv stability; rather, decreases in HSP60 levels in 22Rv1 cells were associated with loss of mitochondrial spare respiratory capacity. The importance of the relationship between HSP60 and CRPC was further validated by analysis of transcriptional data from PCa patient samples, which showed a strong correlation between HSP60 transcript levels and poor disease outcomes. Together, these results identify a potential drug target for the treatment of CRPC as well as more broadly suggest how proteostasis networks might be adapted to provide drug resistance in PCa.

RESULTS

Design of the Proteostasis Library

To explore the chaperone dependence of PCa and CRPC cell lines, we used a focused shRNA library, termed the Proteostasis Library, that targets 139 genes encoding chaperones and related factors (Figure 1A; see below). This library is composed of 25 targeting sequences per gene (listed in Table S1), plus an additional 500 control, non-targeting sequences. These shRNA sequences are cloned into a lentiviral vector and used in a pooled screen format, as previously described (Abrams et al., 2021; Kampmann et al., 2013, 2015). The genes selected for inclusion in this library include examples of the major chaperone families, such as HSP70s, HSP90s, chaperonins (TRiC/CCT and HSP60/HSPD1), and small heat shock proteins (sHSPs) (Figure 1A). It also includes the major co-chaperones for HSP70s, such as J-domain proteins (JDPs, also called HSP40s), tetratricopeptide repeat (TPR) domain proteins and nucleotide-exchange factors (NEFs), and the major co-chaperones for HSP90, such as CDC37, AHA1, and PTGES3 (also called p23). Beyond chaperones, chaperonins, and co-chaperones, the library includes other protein folding and maintenance enzymes, such as protein disulfide isomerases (PDIs), peptidyl prolyl isomerases (PPIases), and factors required for proteasome assembly (e.g., PSMG1) and protein trafficking (e.g., VCP/97, Sec63). Finally, the library covers a subset of targets that are involved in stress signaling pathways, including HSF1/2, ATF6, and XBP1. It is worth noting that although CRISPR/Cas9-based methods are also a powerful alternative way to perform screens, we favored the shRNA approach in this particular case because it can be used in multiple cell lines without the requirement for stable expression of Cas9/dCas9. Together, this shRNA library provides broad coverage of the major functional and regulatory components of the proteostasis network, allowing potential identification of cancer sensitivities across various functions.

In assembling the Proteostasis Library, we favored groups of targets that are known to physically bind to each other (bold and dotted lines in Figure 1A). One of the defining features of the proteostasis network is that many of the components engage in protein-protein interactions (PPIs), both with each other and with their client proteins (Freilich et al., 2018). Another feature of this network is that there is potential redundancy built into it. For example, in human cells, there are genes for ~13 HSP70s, ~50 JDPs, and 6 HSP90s (Chen et al., 2005; Kampinga et al., 2009; Radons, 2016). To illustrate this feature in Figure 1A, we clustered the genes in functional families and depict them as a schematic map that highlights the PPIs. For each class, there are members that are localized to specific sub-cellular locations; for example, the major HSP70s of the cytosol are HSP72 (HSPA1A) and HSC70 (HSPA8), while BiP/HSPA5 and mortalin/HSPA9 are found in the endoplasmic reticulum (ER) and mitochondria, respectively (Rosenzweig et al., 2019).

Functional genomics screen to identify shared and unique vulnerabilities in PCa and CRPC cell lines

Using the Proteostasis Library, we conducted a functional genomics screen by transducing cells with the pooled shRNAs, growing them for 10 doubling times, and then deep sequencing at the initial (T_0) and final (T_{final}) time points (Figure 1B). Results on the individual shRNA level showed that the screens produced viable results and the negative controls behaved as expected (Figure S1). From these results, we determined the phenotype and p value of each gene knockdown (Table S2), as described (Kampmann et al., 2013). Here, phenotype was calculated by comparing the shRNA frequencies at the T_0 and T_{final} time points, along with the cell growth rate, and the Mann-Whitney p value

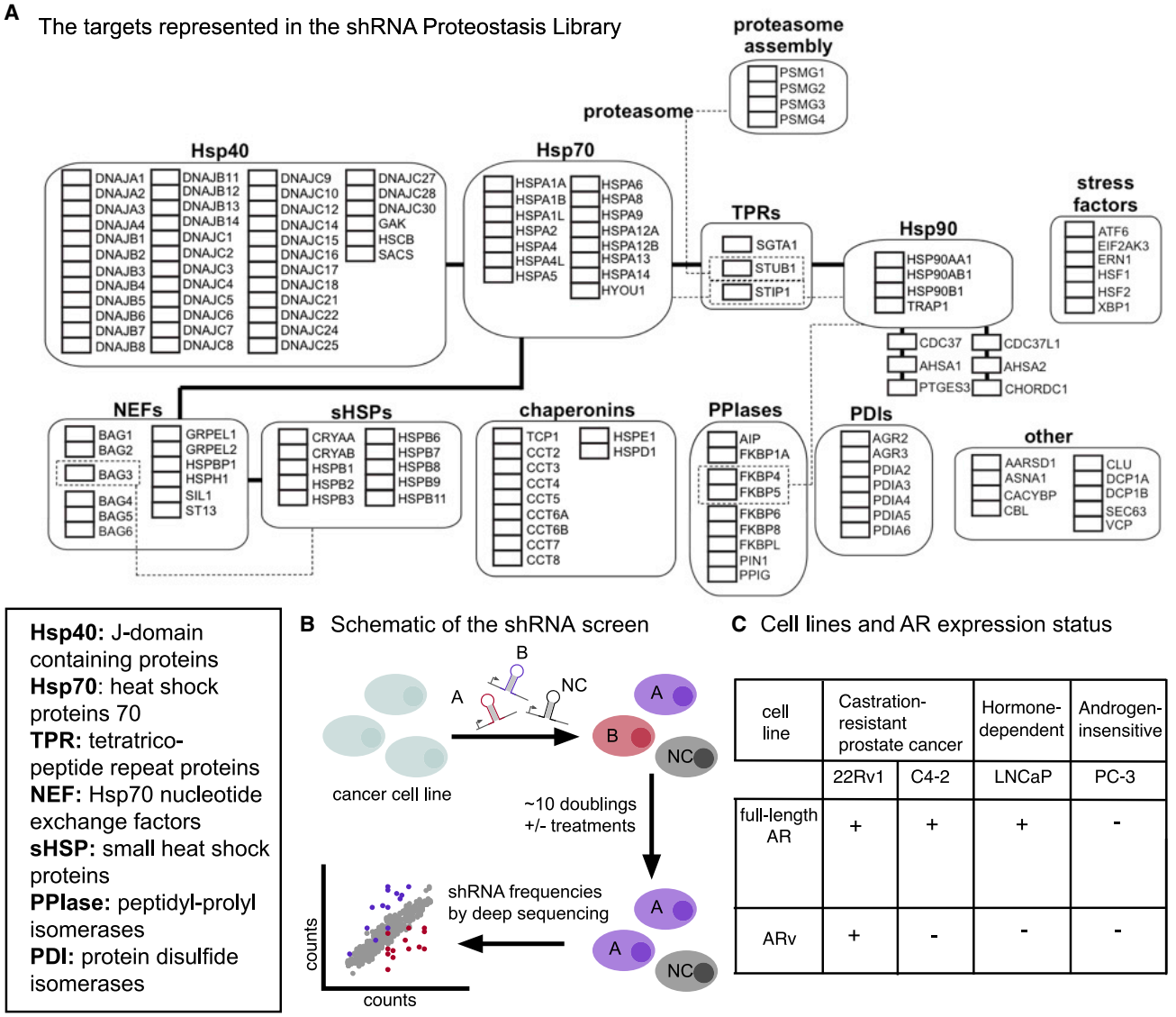

cell line	Castration-resistant prostate cancer		Hormone-dependent	Androgen-insensitive
	22Rv1	C4-2	LNCaP	PC-3
full-length AR	+	+	+	-
ARv	+	-	-	-

Figure 1. Functional genomic screen in PCa cell lines

(A) Map of the chaperones and other proteostasis targets represented in the shRNA Proteostasis Library. Targets are grouped by structural categories (e.g., HSP70s, sHSPs). The bold lines between the categories represent known physical connections (e.g., protein-protein interactions). The dotted lines represent connections that are specific to only the indicated members of the class.

(B) Schematic of the workflow for the functional genomics screen. Cells are transduced with lentivirus expressing targeting (A, B, etc.) and ~500 non-targeting negative control (NC) sequences. After selections performed with or without proteostasis stressors, the enrichment or depletion of specific shRNA sequences is quantified by deep sequencing and comparison of T_0 to T_{final}.

(C) Four prostate cancer cell lines, organized by hormone sensitivity and AR expression status.

was calculated by comparing the results of the 25 shRNAs per gene to the negative control shRNAs.

These screens were conducted in four different cell lines. Two of these lines (22Rv1 and C4-2) are androgen-insensitive CRPC cells. The 22Rv1 cells express both full-length AR and the truncated form (ARv7), whereas the C4-2 cells express only full-length AR. As controls, we performed the screens in two additional PCa cell lines: an AR positive, androgen-sensitive cell line (LNCaP) and an AR-negative cell line (PC3) (Figure 1C). For each of the four cell lines, the screens identified proteostasis factors important for growth (Figure 2A). These factors are highlighted in Figure 2A, but also labeled in bold in Table S2. One of the first observations was that only a small subset of proteostasis factors (~10%) were identified as "hits" in any of the cell lines. This limited sensitivity was most dramatic for the PC3 cell line, where only 4 of 139 (3%) genes were considered "hits" ($p < 0.01$) (Figure 2A). This finding suggests that PC3 cells, and to a lesser extent the other cell lines, can tolerate partial loss of many/most proteostasis factors; however, because this is a pooled screen, it also remains likely that there are false negatives. Regardless, the low percentage of "hits" allowed us to rapidly focus on the most sensitive factors.

A Selective vulnerabilities in CRPC and PCa cell lines, revealed by functional genomic screens

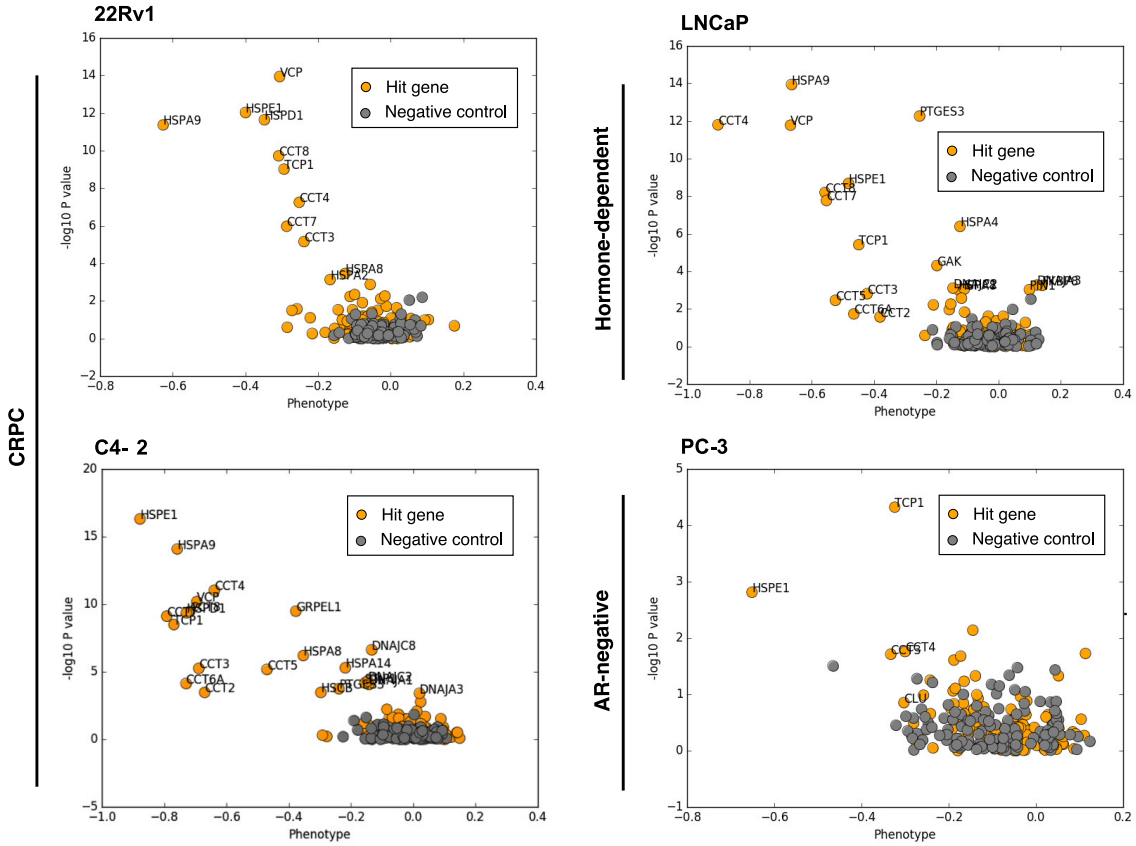

B Prostate cancer cell lines have both shared and distinct vulnerabilities

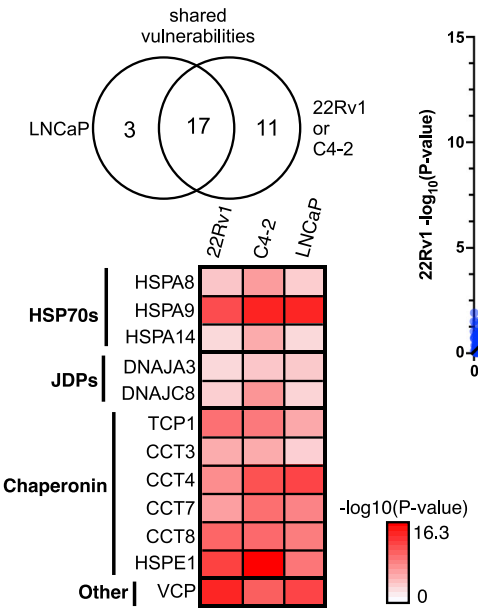

C CRPC cells have unique vulnerabilities vs. LnCaP cells

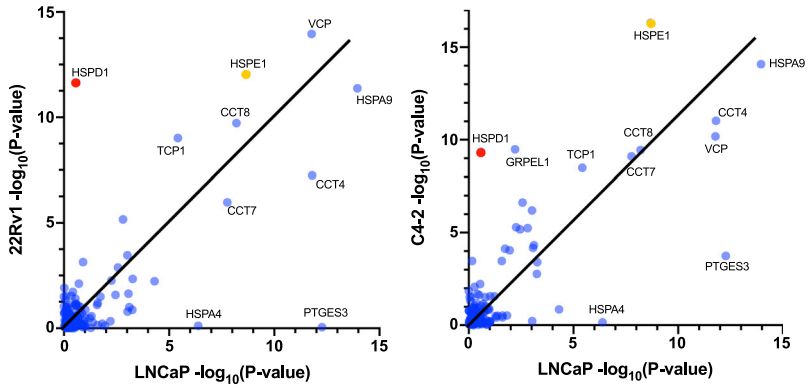

(legend on next page)

To explore the similarities and differences between the cell lines in more detail, we established a cutoff of $p < 0.01$ ($-\log_{10}(p) > 2$) and then combined the vulnerabilities from the CRPC (22Rv1 and C4-2) cell lines and compared them with the LNCaP cell lines. At this point, the PC3 data were excluded owing to the low hit rate. This comparative analysis identified 17 "hits" that are largely shared across the cell lines (e.g., shared vulnerabilities), as well as three unique vulnerabilities for the LNCaP cells and 11 hits unique to CRPC (Figure 2B). The shared vulnerabilities included a subset of HSP70s and HSP40/JDPs as well as TriC/CCT, HSP10 (gene name HSPE1), and VCP/p97 (Figure 2B, heatmap). This result was satisfactory because, as mentioned above, HSP70s, HSP90s, and JDPs have a well-characterized role in AR processing (Echeverria and Picard, 2010; Kirschke et al., 2014; Pratt et al., 2006). Interestingly, these AR processing factors were not identified in the PC3 cell line, which does not express AR or ARv, but were shared in the LNCaP, 22Rv1, and C4-2 cell lines, which do (see Figure 1C). It seems likely that some of the other shared factors are involved in general cancer cell growth and survival, and indeed, VCP/p97 has been previously identified as being broadly important in PCa (Tsujimoto et al., 2004).

Next, to better visualize the selective vulnerabilities, we plotted the $-\log_{10}(p)$ for each gene in the LNCaP experiments versus each of the two CRPC cell lines (Figure 2C). We also plotted the sensitivities onto the shRNA library maps to look for physical/functional relationships (Figure S2). Through this analysis, we observed that the LNCaP cells appear to have a reliance on HSPA4 (an HSP70 isoform) and PTGES3 (p23), the latter of which has been associated with both HSP90-dependent and -independent roles in transcription (Echtenkamp et al., 2011; Freeman et al., 2000). Next, we turned our attention to the factors that were identified as selective vulnerabilities in the CRPC cells. Most strikingly, this analysis showed that 22Rv1 and C4-2 cells depend on the mitochondrial chaperonin, HSP60/HSPD1. HSP60 is known to form a complex in the mitochondria with HSP10/HSPE1, which is a shared hit among all four tested cell lines. The C4-2 cells also relied on GRPEL1, another mitochondria-localized chaperone that is thought to be involved in mitochondrial protein folding and import. Together, these results suggested that CRPC cells have selective vulnerabilities in the proteostasis network and that a number of these cluster to the mitochondrial sub-network.

Synthetic lethality screens with HSP70 and HSP90 inhibitors highlight HSP60 as an important selective vulnerability in CRPC cells

Because HSP70 and HSP90 are known to be involved in AR processing, we wondered whether repeating the shRNA screens in the presence of chemical inhibitors of these chaperones might reveal synthetic lethalities. First, we characterized the effects of these inhibitors on AR and ARv in our hands. Consistent with the literature (Moses et al., 2018), we found that treatment with AUY-922 (an inhibitor of HSP90) (Figure 3A) leads to loss of full length (FL) AR in 22Rv1, LNCaP, and C4-2 after 6 h (Figure 3B). We also confirmed that AUY-922 was unable to affect ARv in 22Rv1 cells. On the other hand, treatment with JG-231 (an inhibitor of HSP70) only mildly reduced FL AR, but was effective in reducing ARv in the 22Rv1 cells (Figure 3B).

Guided by these results, we repeated the shRNA screen in the 22Rv1, C4-2, and LNCaP cell lines in the presence of JG-231 or AUY-922. Cells were treated three times throughout the growth period with either JG-231 or AUY-922, at established concentrations that were found to have anti-proliferative effects while still allowing cells to recover and continue growing (see STAR Methods). Through the calculations described earlier, we determined the phenotype and p value of genetic knockdown in each of these conditions. We found that the main "hits" from these chemical-genetic screens could be binned into three categories—shared, cell-line specific, and drug-treatment specific (Figure 3C). Among the shared and cell-line specific hits, we found that the vulnerabilities were largely similar between the initial screen and the chemical-genetic screen. For example, HSP70 isoforms (gene name HSPA8, HSPA9, HSPA14), the JDPs (DNAJA3, DNAJC8), and the TRiC complex (CCT4, CCT7, CCT8) remain essential in the presence of either inhibitor (Figure 3C). Consistent with this idea, hierarchical clustering revealed overall similar patterns of genetic vulnerabilities (Figure S3). However, novel hits emerged as well. For example, we found that the cytosolic HSP90 gene (HSP90AB1) was essential in the presence of the HSP90 inhibitor (AUY-922) in all three cell lines. Moreover, HSP90AB1 was also essential in 22Rv1 cells after HSP70 inhibition. These strong interactions suggested, perhaps not surprisingly, that the proteostasis network becomes more reliant on HSP90s when this chaperone is partially inhibited. Interestingly, the co-chaperone HOP/STIP1, which is known to bind both HSP70 and HSP90 (Bhattacharya et al., 2020; Johnson et al., 1998), was also required only in the presence of AUY-922. This result suggests that the communication between these chaperones might become more important upon HSP90 inhibition. Another striking finding from this synthetic lethal screen was that HSP60/HSPD1 was again found to be a strong vulnerability only in the 22Rv1 and C4-2 cells, but not in the LNCaP (Figure 3C). Overall, these results validated our previous observations and suggested that HSP60 could be an interesting target in CRPC cells.

HSP60 is a selective vulnerability in CRPC cells

HSP60 is a mitochondrial chaperonin, homologous to the bacterial GroEL, which is involved in mitochondrial protein folding (Bukau and Horwich, 1998; Pace et al., 2013). To validate the HSP60 result from the screen, we transduced 22Rv1, C4-2, LNCaP, and PC3 cells with two different red fluorescent protein (RFP)-labeled shRNAs or a scrambled negative control and selected with

Figure 2. CRPC cell lines have unique vulnerabilities that are distinct from PCa cells

(A) Volcano plots showing the results of the functional genomics screen for each of the four cell lines.

(B) Comparisons between the CRPC cell lines (22Rv1 and C4-2) and the PCa cell lines (LNCaP) reveal both shared and distinct subsets of vulnerabilities. All genes with $-\log10(p) > 2$ in all three cell lines are shown.

(C) To illustrate differences between the LNCaP and CRPC cell lines, the $-\log_{10}(p)$ are plotted against each other, such that those genes far from the diagonal are preferentially required in one cell line and not the other. For reference, HSPD1 is shown in red, and HSPE1 is shown in orange.

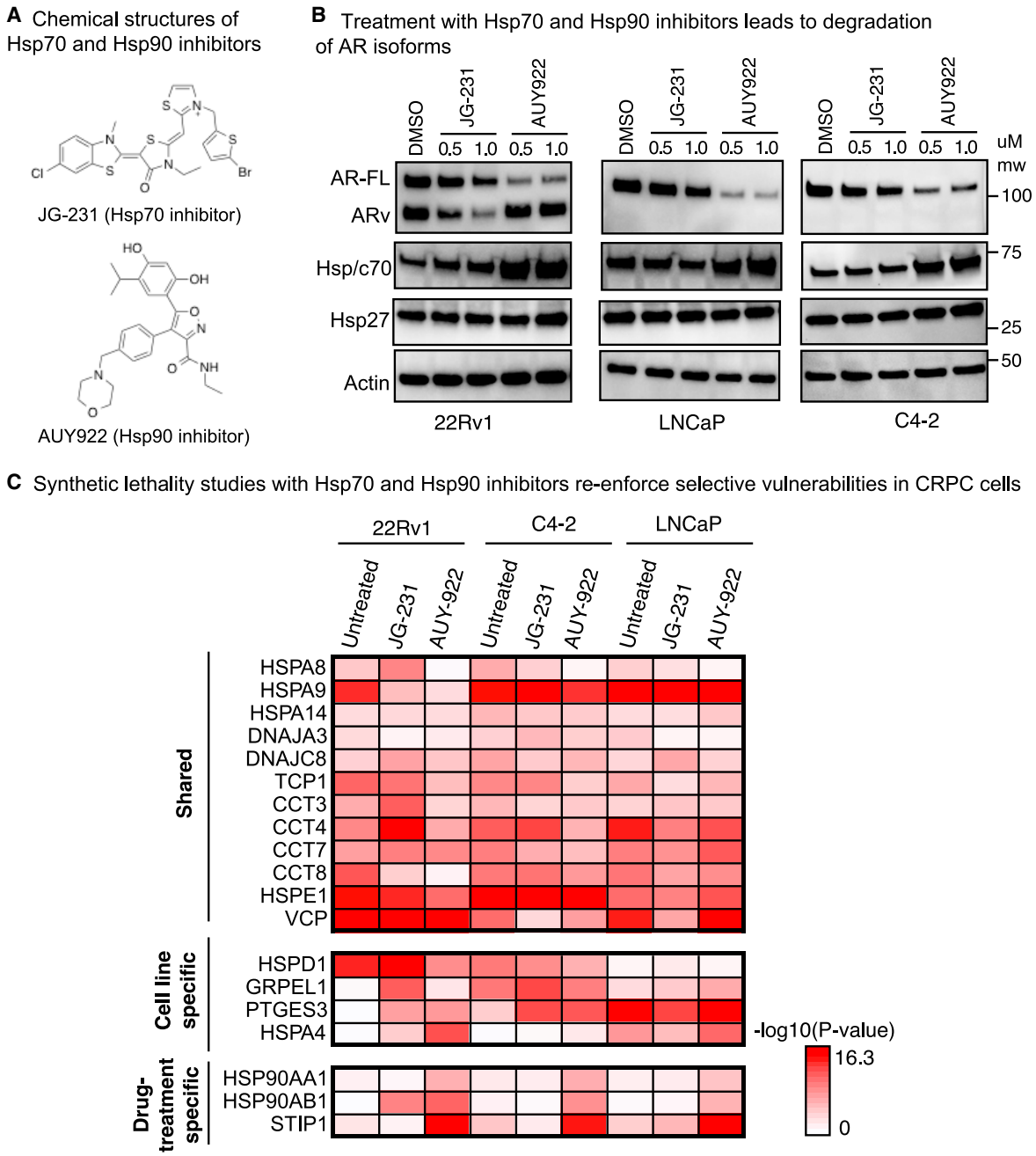

Figure 3. Synthetic lethality studies using chemical inhibitors of HSP70 and HSP90 suggest that CRPC cells depend on HSP60/HSPD1

(A) Chemical structure of the compounds used in this study. JG-231 and AUY-922 are pan-inhibitors of HSP70 and HSP90, respectively.

(B) Treatment with AUY-922 leads to degradation of full-length AR, and treatment with JG-231 leads to degradation of ARv in PCa cell lines. Experiments are representative of studies performed in triplicate.

(C) The p values of selected genes show various patterns of knockdown sensitivity across PCa cells. Shared and cell-line specific hits from the untreated condition generally remain hits with HSP70 and HSP90 inhibition, and some drug-treatment specific sensitivities are revealed.

puromycin. In 22Rv1 cells, knockdown was >90% for both shRNA sequences, but not the control (Figure 4A). The cells were then maintained for 3 weeks, and the percentage of RFP-positive cells was monitored during every passage by flow cytometry (Figure S4). From these studies, we observed depletion of the RFP-positive population in the 22Rv1 (Figure 4B) and C4-2 cells, but not LNCaP or PC-3 cells (Figure 4C). To understand whether this reliance on HSP60 was restricted to CRPC cell lines, we knocked it down in multiple other cancer subtypes, with a focus on breast cancer (MCF7 and MDA-MD-231) and multiple myeloma (KMS-11, KMS-34, OPM-2, AMO-1) cell lines because of their established connections with chaperones and

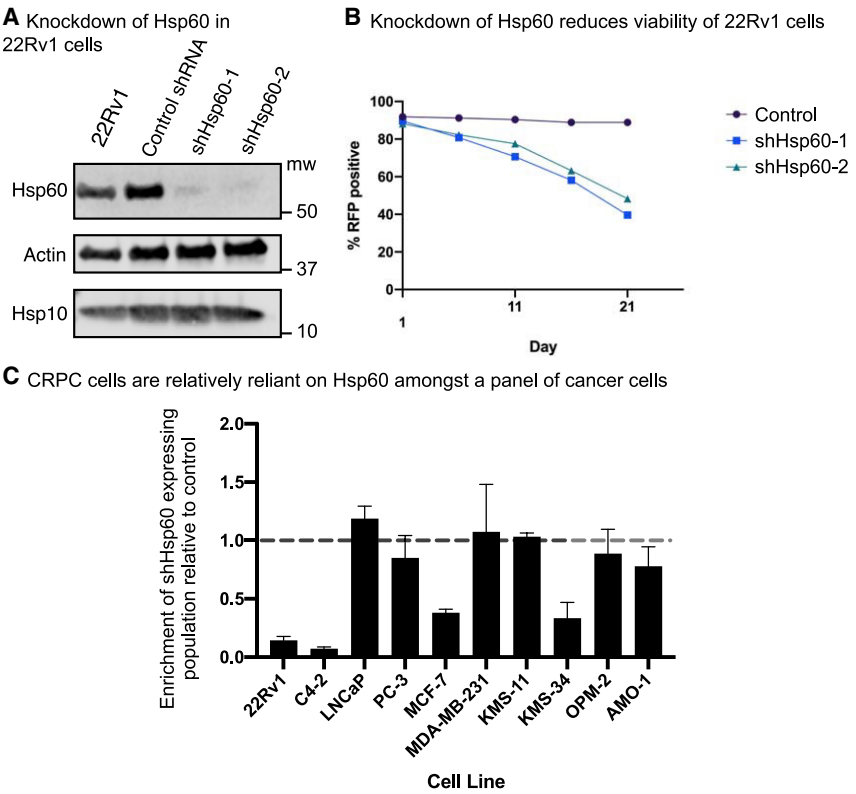

Figure 4. Validation of HSP60 as a selective vulnerability in CRPC cell lines

(A) 22Rv1 cells were transduced with either a control or HSP60 targeting shRNA, which induced robust knockdown (>90%). Results are representative of experiments performed in triplicate.

(B) The shRNA expressing population was monitored via flow cytometry through RFP expression. Over time, the population of HSP60 knockdown cells decreased compared with the control shRNA.

(C) A panel of additional cancer cells were transduced with the HSP60 shRNAs, and the RFP-expressing population was monitored over time (~2–3 weeks). HSP60 knockdown was strongly depleted in CRPC cells (22Rv1 and C4-2), but not in the other tested PCa, breast, or multiple myeloma cells. Enrichment was calculated as the ratio of (RFP+)/(1-RFP+) between the initial and final time points, relative to a control shRNA. Results are the average of two independent experiments, and the error bars represent SD.

proteostasis (Sannino and Brodsky, 2017; Sha and Goldberg, 2020). We found that 4/6 cell lines did not rely on HSP60/HSPD1 for growth (Figures 4C and S4). In 2/6 cell lines (MCF-7 and KMS-34), only a partial decrease (about 50% depletion compared with the control) in the RFP population was observed. Thus, the CRPC cell lines had an unusual, but not entirely exclusive, reliance on HSP60/HSPD1.

HSP60 knockdown does not affect AR levels

While HSP70 and HSP90 directly regulate AR stability (see Figure 3B), we considered it unlikely that HSP60 would operate through a similar mechanism owing to its mitochondrial localization. However, the expression of AR and ARv is known to be sensitive to manipulation of metabolic pathways, such as inhibition of fatty acid metabolism (Schlaepfer et al., 2014; Zadra et al., 2019), so it seemed possible that HSP60 could regulate AR stability through indirect mechanisms. Thus, we examined whether HSP60 knockdown reduced AR levels in the doxycycline (dox)-inducible 22Rv1 cells. These cells were treated with dox for 96 h, which produced a robust knockdown of HSP60 without any impact on AR or ARv (Figure 5A). These results suggest that HSP60 is involved in survival of CRPC cells through a mechanism that is independent of AR stability.

Metabolic effects of HSP60 knockdown

Another possibility is that HSP60 could be important for metabolic reprogramming in CRPC cell lines. To test this idea, we monitored the impact of HSP60 loss on mitochondrial respiration in 22Rv1 cells using the Mito Stress Test (Agilent). In this assay, oligomycin, trifluoromethoxy carbonyl cyanide phenylhydrazone (FCCP), and Rotenone/Antimycin A are sequentially added to cultured cells to calculate mitochondrial activity and capacity (Figure 5B). Upon 5-day treatment with dox, HSP60 knockdown suppressed numerous aspects of mitochondrial respiration. In general, HSP60 loss resulted in lower basal oxygen consumption; however, this effect was relatively minor compared with the decrease in the maximal oxygen consumption rate (OCR) (Figure 5C). Loss of HSP60 consistently reduced the spare respiratory capacity (maximal OCR – basal OCR) of 22Rv1 cells and was generally accompanied by an increase in proton leakage, an indication that the integrity of the electron transport chain (ETC) and/or the inner membrane is disrupted (Figures 5E and 5F). These effects were often accompanied by variable impacts on basal respiration and glycolytic response, indicating that HSP60 is more important in maintaining mitochondrial plasticity than it is in maintaining basal respiration in 22Rv1 cells (Figure 5D). These effects were reproducible with an alternative shRNA sequence, and similar results were observed in independent replicates (Figure S5).

Clinical significance of HSP60 in CRPC

Lastly, we wanted to examine if HSP60 expression had a clinical correlation to patient outcomes in PCa, especially in patients who had been previously treated with ADT. Toward that goal, we analyzed metastasis-free survival in ADT-treated (n = 243) and non-ADT-treated (n = 476) patients from the Decipher GRID database, which were pooled from two matched cohorts previously (Karnes et al., 2018), and compared them based on HSP60/HSPD1 gene transcript levels. Here, high HSP60 expression was defined as greater than the median of all patients. Strikingly, ADT-treated patients with high HSP60 expression had significantly worse outcomes (hazard ratio [HR] = 1.95, p = 0.00024) (Figure 6). Among the patients who had not received ADT (no-ADT), those with high HSP60 expression have slightly worse metastasis-free survival outcomes (HR = 1.4), but this

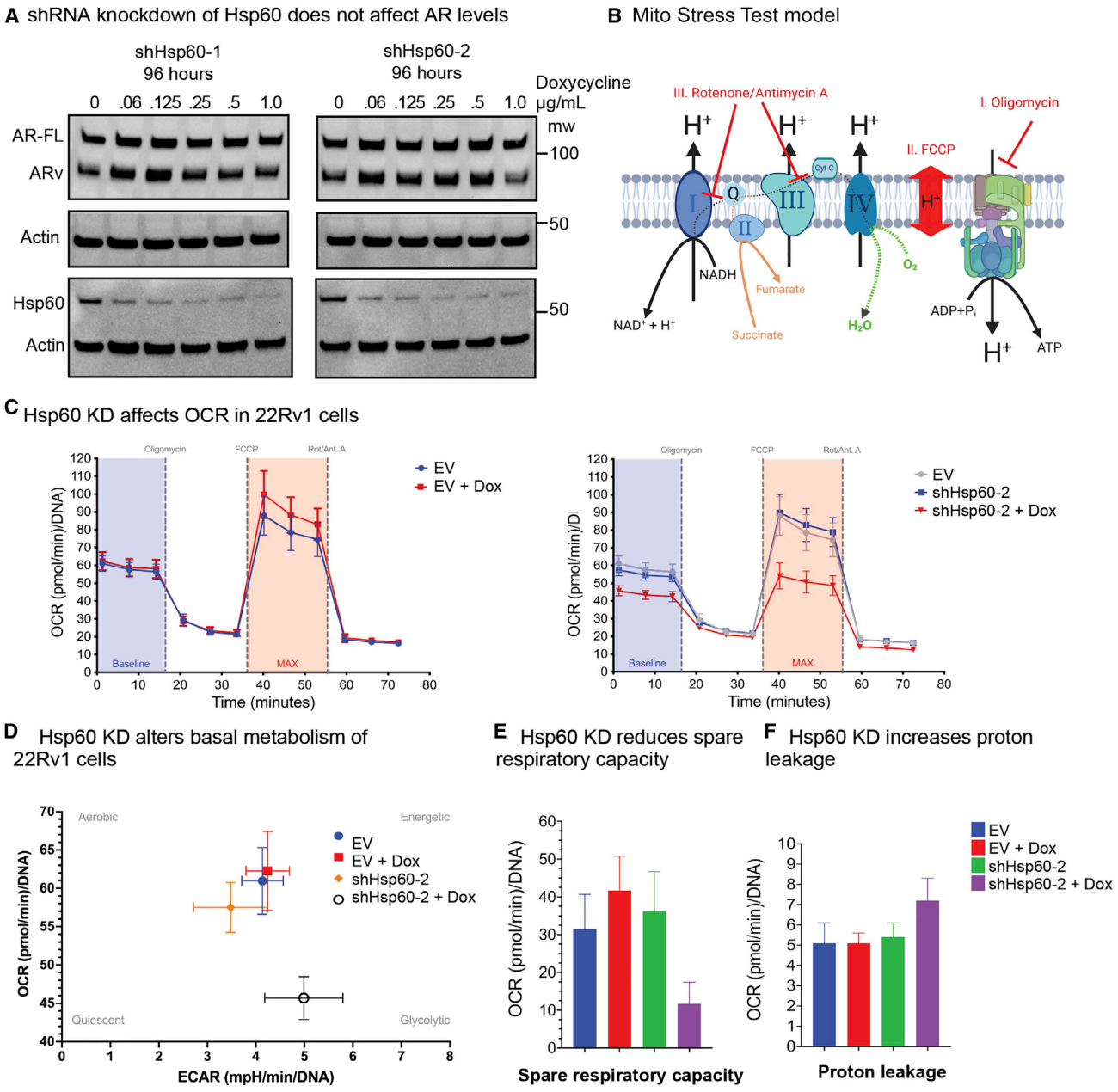

Figure 5. HSP60 knockdown does not affect AR, but HSP60 promotes mitochondrial respiration of 22Rv1 cells

(A) Dox-inducible shRNAs of HSP60 were stably expressed in 22Rv1 cells. shRNAs reduce HSP60 levels, but both full-length and ARv levels are unaffected after 96 h of dox treatment.

(B) Model of Mito Stress Test overlaid on inner mitochondrial membrane and ETC.

(C) Mito Stress Test analysis of 22Rv1 EV or dox-inducible shHSP60-2 with and without 5 days treatment with 100 ng/mL doxycycline.

(D) Energetic plot of basal metabolism of 22Rv1 EV or shHSP60-2 cells with and without dox.

(E and F) Quantitation of spare respiratory capacity or (F) proton leakage of 22Rv1 EV or HSP60-3 with and without 5 days treatment with 100 ng/mL doxycycline. Results are the average of three technical replicates (n = 3), and error bars represent SEM. In addition, the results are representative of an independent replicate (see Figure S5B), and similar results were obtained with a second shRNA sequence (see Figure S5A).

finding was not statistically significant (p = 0.02). These findings suggest that high HSP60 levels correlate with worse metastasis-free survival in PCa patients, especially in patients who were previously treated with ADT. This result is consistent with the idea that HSP60 is especially important in CRPC cells.

DISCUSSION

Given the established dependence of PCa cells on AR signaling, the proteostasis network has been suggested to contain putative drug targets (Ballar Kirmizibayrak et al., 2020). Here, we used

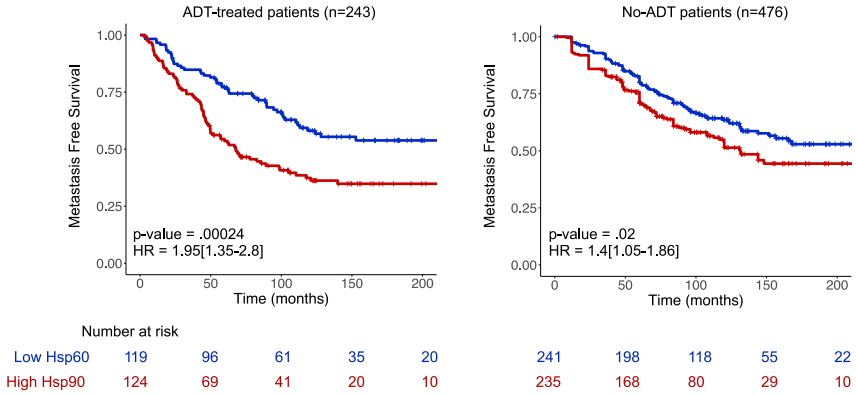

Figure 6. Comparison of metastasis-free survival in patients with high (red, greater than median expression) or low (blue, lower than median expression) HSP60 expression, with or without ADT treatment. HSP60 expression significantly correlates with worse outcomes in ADT-treated PCa patients. See the text for additional details.

focused shRNA screens to search for additional proteostasis factors that might be required for cell growth and survival in CRPC and PCa cell lines. Through these studies, we discovered "hits" that are shared among all the cell lines, such as the TriC/CCT complex, VCP/p97, and HSP10. Both TriC/CCT and VCP/p97 have been broadly implicated in tumorigenesis (Anderson et al., 2015; Boudiaf-Benmammar et al., 2013), so this shared dependence was consistent with probable roles in sustaining general cancer phenotypes, such as rapid growth and proliferation. Here, we were more interested in factors that were selective for growth of CRPC cell lines. Among the findings, we became most interested in HSP60/HSPD1, which was identified as a strong hit only in the CRPC cell lines (22Rv1 and C4-2). This chaperonin had previously been linked to clinical PCa (Beyene et al., 2018; Castilla et al., 2010), so this finding seemed most promising.

HSP60 is known to be involved in mitochondrial protein folding and translocation (Bukau and Horwich, 1998; Cheng et al., 1989; Pace et al., 2013). It has been shown to have various roles in cancer, such as glioblastoma (Polson et al., 2018; Tang et al., 2016) and non-small cell lung cancer (NSCLC) (Parma et al., 2021), but its exact function has not been determined. Proteomics studies have identified a number of substrates of HSP60, including malate dehydrogenase and other tricarboxylic acid (TCA) cycle-related proteins (Bie et al., 2020). We found that knockdown of HSP60/HSPD1 does not affect AR levels, but rather has a strong effect on mitochondrial spare respiratory capacity (see Figure 5D). Spare respiratory capacity is a strong predictor of metastatic potential, given that it is related to a cell's ability to respond to diverse stress stimuli (Marchetti et al., 2020). As cancer cells escape their tissue of origin, they encounter environments that differ substantially from the nutritional characteristics to which they are accustomed. Spare respiratory capacity likely plays an important role in supporting the ability of foreign cells to thrive in such environments, thereby promoting the ability of PCa to escape its natural environment and thrive in foreign nutrient environments. Our results support a model in which PCa becomes increasingly reliant on HSP60 as it deviates from androgen-dependent growth and escapes the prostate. By promoting the activity of components of the ETC, HSP60 helps CRPC cells resist the stress related to metastatic growth. In general support of this idea, HSP60 has recently been found to regulate oxidative phosphorylation in NSCLC cells through effects on cytochrome *c* oxidase and the creatine transporter SLC6A8 (Parma et al., 2021). In addition, knockdown of HSP60 has recently been shown to activate autophagy in adipose tissue (Hauffe et al., 2021), and treatment with an HSP60 inhibitor induces autophagy in glioblastoma cells (Polson et al., 2018). This autophagy induction could be a compensatory response to delay apoptosis. This relationship between HSP60, metabolism, and cell survival appears to be important in patients, as we observed in clinical data that low HSP60 expression significantly correlates with metastasis-free survival in prostate tumors from patients treated with ADT. Moreover, HSP60 is upregulated after 8 weeks in a mouse model of CRPC development (Akamatsu et al., 2015). These findings generally agree with our *in vitro* observations that HSP60 plays a special role in CRPC cell lines, but not LNCaP or PC3. HSP60 (and its prokaryotic ortholog, GroEL) has been the target of multiple drug discovery and chemical biology campaigns (Chapman et al., 2009; Polson et al., 2018; Shao et al., 2020; Stevens et al., 2020; Wiechmann et al., 2017). The present study suggests that CRPC might be a promising disease target for these emerging inhibitors.

More broadly, it seems likely that the proteostasis networks of PCa cells are re-programmed during disease progression and the onset of ADT resistance. Thus, whether an inhibitor of proteostasis works for a specific PCa stage might depend on multiple factors, including the prior treatment regimen. Functional genetic tools such as the Proteostasis Library, plus other biochemical technologies (Rizzolo et al., 2017; Rodina et al., 2016; Taipale et al., 2014), may begin to unravel these selective vulnerabilities for PCa and other indications.

SIGNIFICANCE

Prostate cancer (PCa) is among the most common cancers in men. While treatments for early stages of this disease are effective, there is an urgent need for better treatments in the advanced stages, such as castration-resistant prostate cancer (CRPC). The molecular chaperones, such as HSP70 and HSP90, have been closely linked to PCa and CRPC because of their ability to stabilize the androgen receptor (AR) and its variants. Here, we used a functional genomics approach to reveal whether other chaperones might also be important for survival of CRPC cells. Specifically, we performed screens in four PCa and CRPC cell lines, using shRNA libraries targeting ~140 chaperones, chaperonins, co-chaperones, and related proteins. We also repeated the screens using chemical inhibitors of HSP70 and HSP90 to reveal potential synthetic lethality relationships. The results

suggest that HSP60 is a promising drug target for CRPC, a finding that is supported by evidence for high HSP60 transcript levels in patients. These results are significant because they provide support for a potential treatment strategy. More broadly, the work illustrates a way to identify selective vulnerabilities and synthetic lethal relationships in cancer and other diseases, using focused shRNA libraries in combination with chemical inhibitors of key proteostasis nodes.

STAR★METHODS

Detailed methods are provided in the online version of this paper and include the following:

- KEY RESOURCES TABLE
- RESOURCE AVAILABILITY
  - Lead contact
  - Materials availability
  - Data and code availability
- EXPERIMENTAL MODEL AND SUBJECT DETAILS
  - Cell lines
  - Lentiviral production and transduction
- METHOD DETAILS
  - Reagents
  - Pooled shRNA screens and individual shRNA validation
  - Genomic DNA isolation, indexing and PCR purification
  - Mito stress test
  - Data analysis and clustering
  - Immunoblotting
  - Clinical data analysis
- QUANTIFICATION AND STATISTICAL ANALYSIS

SUPPLEMENTAL INFORMATION

Supplemental information can be found online at https://doi.org/10.1016/j.chembiol.2022.01.008.

ACKNOWLEDGMENTS

This work was supported by grants from StandUp2Cancer (J.E.G. and M.K.), the US Department of Defense PC150065 Idea Development Award (J.E.G. and L.N.), NIH/NCI CA181494 (M.K.), and the Stephen and Nancy Grand Multiple Myeloma Translational Initiative (M.K.). L.N., F.E., M.A.M., and G.M.R.-M. were supported with funds from the Intramural Program, Center for Cancer Research, National Cancer Institute, to L.N. under Investigator Initiated Project Number ZIA SC 010074.

AUTHOR CONTRIBUTIONS

A.S., I.R.T., F.E., P.R., M.A., G.M.R.-M., M.A.M., and H.S. designed and conducted experiments and interpreted results. R.J.K., L.N., F.F., M.K., and J.E.G. interpreted results and provided resources. A.S., I.R.T., and J.E.G. prepared the manuscript, with assistance from the other authors.

DECLARATION OF INTERESTS

J.E.G. holds patents to the use of HSP70 inhibitors and is a member of the Cell Chemical Biology Scientific Advisory Board. The authors declare no other competing interests.

Received: June 21, 2021
Revised: September 17, 2021
Accepted: January 11, 2022
Published: February 1, 2022

REFERENCES

Abrams, J., Arhar, T., Mok, S.A., Taylor, I.R., Kampmann, M., and Gestwicki, J.E. (2021). Functional genomics screen identifies proteostasis targets that modulate prion protein (PrP) stability. Cell Stress Chaperones *26*, 443–452.

Akamatsu, S., Wyatt, A.W., Lin, D., Lysakowski, S., Zhang, F., Kim, S., Tse, C., Wang, K., Mo, F., Haegert, A., et al. (2015). The placental gene PEG10 promotes progression of neuroendocrine prostate cancer. Cell Rep. *12*, 922–936.

Anderson, D.J., Le Moigne, R., Djakovic, S., Kumar, B., Rice, J., Wong, S., Wang, J., Yao, B., Valle, E., Kiss von Soly, S., et al. (2015). Targeting the AAA ATPase p97 as an approach to treat cancer through disruption of protein homeostasis. Cancer Cell *28*, 653–665.

Antonarakis, E.S., Lu, C., Wang, H., Luber, B., Nakazawa, M., Roeser, J.C., Chen, Y., Mohammad, T.A., Chen, Y., Fedor, H.L., et al. (2014). AR-V7 and resistance to enzalutamide and abiraterone in prostate cancer. N. Engl. J. Med. *371*, 1028–1038.

Arora, V.K., Schenkein, E., Murali, R., Subudhi, S.K., Wongvipat, J., Balbas, M.D., Shah, N., Cai, L., Efstathiou, E., Logothetis, C., et al. (2013). Glucocorticoid receptor confers resistance to antiandrogens by bypassing androgen receptor blockade. Cell *155*, 1309–1322.

Balch, W.E., Morimoto, R.I., Dillin, A., and Kelly, J.W. (2008). Adapting proteostasis for disease intervention. Science *319*, 916–919.

Ballar Kirmizibayrak, P., Erbaykent-Tepedelen, B., Gozen, O., and Erzurumlu, Y. (2020). Divergent modulation of proteostasis in prostate cancer. Adv. Exp. Med. Biol. *1233*, 117–151.

Beyene, D.A., Naab, T.J., Kanarek, N.F., Apprey, V., Esnakula, A., Khan, F.A., Blackman, M.R., Brown, C.A., and Hudson, T.S. (2018). Differential expression of Annexin 2, SPINK1, and Hsp60 predict progression of prostate cancer through bifurcated WHO Gleason score categories in African American men. Prostate *78*, 801–811.

Bhattacharya, K., Weidenauer, L., Luengo, T.M., Pieters, E.C., Echeverria, P.C., Bernasconi, L., Wider, D., Sadian, Y., Koopman, M.B., Villemin, M., et al. (2020). The Hsp70-Hsp90 co-chaperone Hop/Stip1 shifts the proteostatic balance from folding towards degradation. Nat. Commun. *11*, 5975.

Bie, A.S., Comert, C., Korner, R., Corydon, T.J., Palmfeldt, J., Hipp, M.S., Hartl, F.U., and Bross, P. (2020). An inventory of interactors of the human HSP60/HSP10 chaperonin in the mitochondrial matrix space. Cell Stress Chaperones *25*, 407–416.

Boudiaf-Benmammar, C., Cresteil, T., and Melki, R. (2013). The cytosolic chaperonin CCT/TRiC and cancer cell proliferation. PLoS ONE *8*, e60895.

Brodsky, J.L., and Chiosis, G. (2006). Hsp70 molecular chaperones: emerging roles in human disease and identification of small molecule modulators. Curr. Top. Med. Chem. *6*, 1215–1225.

Bukau, B., and Horwich, A.L. (1998). The Hsp70 and Hsp60 chaperone machines. Cell *92*, 351–366.

Calderwood, S.K., and Gong, J. (2016). Heat shock proteins promote cancer: it's a protection racket. Trends Biochem. Sci. *41*, 311–323.

Castilla, C., Congregado, B., Conde, J.M., Medina, R., Torrubia, F.J., Japon, M.A., and Saez, C. (2010). Immunohistochemical expression of Hsp60 correlates with tumor progression and hormone resistance in prostate cancer. Urology *76*, 1016–1017.e1.

Chapman, E., Farr, G.W., Furtak, K., and Horwich, A.L. (2009). A small molecule inhibitor selective for a variant ATP-binding site of the chaperonin GroEL. Bioorg. Med. Chem. Lett. *19*, 811–813.

Chaudhury, S., Welch, T.R., and Blagg, B.S. (2006). Hsp90 as a target for drug development. ChemMedChem *1*, 1331–1340.

Chen, B., Piel, W.H., Gui, L., Bruford, E., and Monteiro, A. (2005). The HSP90 family of genes in the human genome: insights into their divergence and evolution. Genomics *86*, 627–637.

Chen, L., Li, J., Farah, E., Sarkar, S., Ahmad, N., Gupta, S., Larner, J., and Liu, X. (2016). Cotargeting HSP90 and its client proteins for treatment of prostate cancer. Mol. Cancer Ther. *15*, 2107–2118.

Cheng, M.Y., Hartl, F.U., Martin, J., Pollock, R.A., Kalousek, F., Neupert, W., Hallberg, E.M., Hallberg, R.L., and Horwich, A.L. (1989). Mitochondrial heat-shock protein hsp60 is essential for assembly of proteins imported into yeast mitochondria. Nature *337*, 620–625.

Crawford, L.J., Walker, B., and Irvine, A.E. (2011). Proteasome inhibitors in cancer therapy. J. Cel. Commun. Signal. *5*, 101–110.

De Leon, J.T., Iwai, A., Feau, C., Garcia, Y., Balsiger, H.A., Storer, C.L., Suro, R.M., Garza, K.M., Lee, S., Kim, Y.S., et al. (2011). Targeting the regulation of androgen receptor signaling by the heat shock protein 90 cochaperone FKBP52 in prostate cancer cells. Proc. Natl. Acad. Sci. U. S. A. *108*, 11878–11883.

Dong, J., Wu, Z., Wang, D., Pascal, L.E., Nelson, J.B., Wipf, P., and Wang, Z. (2019). Hsp70 binds to the androgen receptor N-terminal domain and modulates the receptor function in prostate cancer cells. Mol. Cancer Ther. *18*, 39–50.

Echeverria, P.C., and Picard, D. (2010). Molecular chaperones, essential partners of steroid hormone receptors for activity and mobility. Biochim. Biophys. Acta *1803*, 641–649.

Echtenkamp, F.J., Zelin, E., Oxelmark, E., Woo, J.I., Andrews, B.J., Garabedian, M., and Freeman, B.C. (2011). Global functional map of the p23 molecular chaperone reveals an extensive cellular network. Mol. Cell *43*, 229–241.

Eftekharzadeh, B., Banduseela, V.C., Chiesa, G., Martinez-Cristobal, P., Rauch, J.N., Nath, S.R., Schwarz, D.M.C., Shao, H., Marin-Argany, M., Di Sanza, C., et al. (2019). Hsp70 and Hsp40 inhibit an inter-domain interaction necessary for transcriptional activity in the androgen receptor. Nat. Commun. *10*, 3562.

Eisen, M.B., Spellman, P.T., Brown, P.O., and Botstein, D. (1998). Cluster analysis and display of genome-wide expression patterns. Proc. Natl. Acad. Sci. U. S. A. *95*, 14863–14868.

Freeman, B.C., Felts, S.J., Toft, D.O., and Yamamoto, K.R. (2000). The p23 molecular chaperones act at a late step in intracellular receptor action to differentially affect ligand efficacies. Genes Dev. *14*, 422–434.

Freilich, R., Arhar, T., Abrams, J.L., and Gestwicki, J.E. (2018). Protein-protein interactions in the molecular chaperone network. Acc. Chem. Res. *51*, 940–949.

Gabai, V.L., Yaglom, J.A., Wang, Y., Meng, L., Shao, H., Kim, G., Colvin, T., Gestwicki, J., and Sherman, M.Y. (2016). Anticancer effects of targeting Hsp70 in tumor stromal cells. Cancer Res. *76*, 5926–5932.

Grasso, C.S., Wu, Y.M., Robinson, D.R., Cao, X., Dhanasekaran, S.M., Khan, A.P., Quist, M.J., Jing, X., Lonigro, R.J., Brenner, J.C., et al. (2012). The mutational landscape of lethal castration-resistant prostate cancer. Nature *487*, 239–243.

Hauffe, R., Rath, M., Schell, M., Ritter, K., Kappert, K., Deubel, S., Ott, C., Jahnert, M., Jonas, W., Schurmann, A., et al. (2021). HSP60 reduction protects against diet-induced obesity by modulating energy metabolism in adipose tissue. Mol. Metab. *53*, 101276.

Heinlein, C.A., and Chang, C. (2004). Androgen receptor in prostate cancer. Endocr. Rev. *25*, 276–308.

Johnson, B.D., Schumacher, R.J., Ross, E.D., and Toft, D.O. (1998). Hop modulates Hsp70/Hsp90 interactions in protein folding. J. Biol. Chem. *273*, 3679–3686.

Kampinga, H.H., Hageman, J., Vos, M.J., Kubota, H., Tanguay, R.M., Bruford, E.A., Cheetham, M.E., Chen, B., and Hightower, L.E. (2009). Guidelines for the nomenclature of the human heat shock proteins. Cell Stress Chaperones *14*, 105–111.

Kampmann, M., Bassik, M.C., and Weissman, J.S. (2013). Integrated platform for genome-wide screening and construction of high-density genetic interaction maps in mammalian cells. Proc. Natl. Acad. Sci. U. S. A. *110*, E2317–E2326.

Kampmann, M., Horlbeck, M.A., Chen, Y., Tsai, J.C., Bassik, M.C., Gilbert, L.A., Villalta, J.E., Kwon, S.C., Chang, H., Kim, V.N., et al. (2015). Next-generation libraries for robust RNA interference-based genome-wide screens. Proc. Natl. Acad. Sci. U. S. A. *112*, E3384–E3391.

Karnes, R.J., Sharma, V., Choeurng, V., Ashab, H.A., Erho, N., Alshalalfa, M., Trock, B., Ross, A., Yousefi, K., Tsai, H., et al. (2018). Development and validation of a prostate cancer genomic signature that predicts early ADT treatment response following radical prostatectomy. Clin. Cancer Res. *24*, 3908–3916.

Kirby, M., Hirst, C., and Crawford, E.D. (2011). Characterising the castration-resistant prostate cancer population: a systematic review. Int. J. Clin. Pract. *65*, 1180–1192.

Kirschke, E., Goswami, D., Southworth, D., Griffin, P.R., and Agard, D.A. (2014). Glucocorticoid receptor function regulated by coordinated action of the Hsp90 and Hsp70 chaperone cycles. Cell *157*, 1685–1697.

Logothetis, C.J., Gallick, G.E., Maity, S.N., Kim, J., Aparicio, A., Efstathiou, E., and Lin, S.H. (2013). Molecular classification of prostate cancer progression: foundation for marker-driven treatment of prostate cancer. Cancer Discov. *3*, 849–861.

Luo, J., Solimini, N.L., and Elledge, S.J. (2009). Principles of cancer therapy: oncogene and non-oncogene addiction. Cell *136*, 823–837.

Marchetti, P., Fovez, Q., Germain, N., Khamari, R., and Kluza, J. (2020). Mitochondrial spare respiratory capacity: mechanisms, regulation, and significance in non-transformed and cancer cells. FASEB J. *34*, 13106–13124.

Massie, C.E., Lynch, A., Ramos-Montoya, A., Boren, J., Stark, R., Fazli, L., Warren, A., Scott, H., Madhu, B., Sharma, N., et al. (2011). The androgen receptor fuels prostate cancer by regulating central metabolism and biosynthesis. EMBO J. *30*, 2719–2733.

Montgomery, R.B., Mostaghel, E.A., Vessella, R., Hess, D.L., Kalhorn, T.F., Higano, C.S., True, L.D., and Nelson, P.S. (2008). Maintenance of intratumoral androgens in metastatic prostate cancer: a mechanism for castration-resistant tumor growth. Cancer Res. *68*, 4447–4454.

Moses, M.A., Kim, Y.S., Rivera-Marquez, G.M., Oshima, N., Watson, M.J., Beebe, K., Wells, C., Lee, S., Zuehlke, A.D., Shao, H., et al. (2018). Targeting the Hsp40/Hsp70 chaperone axis as a novel strategy to treat castration-resistant prostate cancer. Cancer Res. *78*, 4022–4035.

Nagel, R., Semenova, E.A., and Berns, A. (2016). Drugging the addict: non-oncogene addiction as a target for cancer therapy. EMBO Rep. *17*, 1516–1531.

Pace, A., Barone, G., Lauria, A., Martorana, A., Piccionello, A.P., Pierro, P., Terenzi, A., Almerico, A.M., Buscemi, S., Campanella, C., et al. (2013). Hsp60, a novel target for antitumor therapy: structure-function features and prospective drugs design. Curr. Pharm. Des. *19*, 2757–2764.

Parma, B., Ramesh, V., Naidu Gollavilli, P., Siddiqui, A., Pinna, L., Schwab, A., Marshall, S., Zhang, S., Pilarsky, C., Napoli, F., et al. (2021). Metabolic impairment of non-small cell lung cancers by mitochondrial HSPD1 targeting. J. Exp. Clin. Cancer Res. *40*, 248–268.

Polson, E.S., Kuchler, V.B., Abbosh, C., Ross, E.M., Mathew, R.K., Beard, H.A., da Silva, B., Holding, A.N., Ballereau, S., Chuntharpursat-Bon, E., et al. (2018). KHS101 disrupts energy metabolism in human glioblastoma cells and reduces tumor growth in mice. Sci. Transl. Med. *10*, eaar2718.

Powers, M.V., Clarke, P.A., and Workman, P. (2009). Death by chaperone: HSP90, HSP70 or both? Cell Cycle *8*, 518–526.

Pratt, W.B., Morishima, Y., Murphy, M., and Harrell, M. (2006). Chaperoning of glucocorticoid receptors. Handb. Exp. Pharmacol. *172*, 111–138.

Pratt, W.B., and Toft, D.O. (2003). Regulation of signaling protein function and trafficking by the hsp90/hsp70-based chaperone machinery. Exp. Biol. Med. *228*, 111–133.

Puhr, M., Hoefer, J., Eigentler, A., Ploner, C., Handle, F., Schaefer, G., Kroon, J., Leo, A., Heidegger, I., Eder, I., et al. (2018). The glucocorticoid receptor is a key player for prostate cancer cell survival and a target for improved antiandrogen therapy. Clin. Cancer Res. *24*, 927–938.

Quigley, D.A., Dang, H.X., Zhao, S.G., Lloyd, P., Aggarwal, R., Alumkal, J.J., Foye, A., Kothari, V., Perry, M.D., Bailey, A.M., et al. (2018). Genomic hallmarks and structural variation in metastatic prostate cancer. Cell *175*, 889.

Radons, J. (2016). The human HSP70 family of chaperones: where do we stand? Cell Stress Chaperones *21*, 379–404.

Rizzolo, K., Huen, J., Kumar, A., Phanse, S., Vlasblom, J., Kakihara, Y., Zeineddine, H.A., Minic, Z., Snider, J., Wang, W., et al. (2017). Features of the chaperone cellular network revealed through systematic interaction mapping. Cell Rep. *20*, 2735–2748.

Rodina, A., Wang, T., Yan, P., Gomes, E.D., Dunphy, M.P., Pillarsetty, N., Koren, J., Gerecitano, J.F., Taldone, T., Zong, H., et al. (2016). The epichaperome is an integrated chaperome network that facilitates tumour survival. Nature *538*, 397–401.

Rosenzweig, R., Nillegoda, N.B., Mayer, M.P., and Bukau, B. (2019). The Hsp70 chaperone network. Nat. Rev. Mol. Cell Biol. *20*, 665–680.

Saldanha, A.J. (2004). Java Treeview–extensible visualization of microarray data. Bioinformatics *20*, 3246–3248.

Sannino, S., and Brodsky, J.L. (2017). Targeting protein quality control pathways in breast cancer. BMC Biol. *15*, 109.

Schlaepfer, I.R., Rider, L., Rodrigues, L.U., Gijon, M.A., Pac, C.T., Romero, L., Cimic, A., Sirintrapun, S.J., Glode, L.M., Eckel, R.H., et al. (2014). Lipid catabolism via CPT1 as a therapeutic target for prostate cancer. Mol. Cancer Ther. *13*, 2361–2371.

Sha, Z., and Goldberg, A.L. (2020). Multiple myeloma cells are exceptionally sensitive to heat shock, which overwhelms their proteostasis network and induces apoptosis. Proc. Natl. Acad. Sci. U. S. A. *117*, 21588–21597.

Shao, H., Li, X., Moses, M.A., Gilbert, L.A., Kalyanaraman, C., Young, Z.T., Chernova, M., Journey, S.N., Weissman, J.S., Hann, B., et al. (2018). Exploration of benzothiazole-rhodacyanines as allosteric inhibitors of protein-protein interactions with heat shock protein 70 (Hsp70). J. Med. Chem. *61*, 6163–6177.

Shao, H., Oltion, K., Wu, T., and Gestwicki, J.E. (2020). Differential scanning fluorimetry (DSF) screen to identify inhibitors of Hsp60 protein-protein interactions. Org. Biomol. Chem. *18*, 4157–4163.

Stevens, M., Howe, C., Ray, A.M., Washburn, A., Chitre, S., Sivinski, J., Park, Y., Hoang, Q.Q., Chapman, E., and Johnson, S.M. (2020). Analogs of nitrofuran antibiotics are potent GroEL/ES inhibitor pro-drugs. Bioorg. Med. Chem. *28*, 115710.

Taipale, M., Tucker, G., Peng, J., Krykbaeva, I., Lin, Z.Y., Larsen, B., Choi, H., Berger, B., Gingras, A.C., and Lindquist, S. (2014). A quantitative chaperone interaction network reveals the architecture of cellular protein homeostasis pathways. Cell *158*, 434–448.

Tang, H., Li, J., Liu, X., Wang, G., Luo, M., and Deng, H. (2016). Down-regulation of HSP60 suppresses the proliferation of glioblastoma cells via the ROS/AMPK/mTOR pathway. Sci. Rep. *6*, 28388.

Tsujimoto, Y., Tomita, Y., Hoshida, Y., Kono, T., Oka, T., Yamamoto, S., Nonomura, N., Okuyama, A., and Aozasa, K. (2004). Elevated expression of valosin-containing protein (p97) is associated with poor prognosis of prostate cancer. Clin. Cancer Res. *10*, 3007–3012.

Watson, P.A., Arora, V.K., and Sawyers, C.L. (2015). Emerging mechanisms of resistance to androgen receptor inhibitors in prostate cancer. Nat. Rev. *15*, 701–711.

Whitesell, L., and Lindquist, S.L. (2005). HSP90 and the chaperoning of cancer. Nat. Rev. *5*, 761–772.

Wiechmann, K., Muller, H., Konig, S., Wielsch, N., Svatos, A., Jauch, J., and Werz, O. (2017). Mitochondrial chaperonin HSP60 is the apoptosis-related target for myrtucommulone. Cell Chem. Biol. *24*, 614–623.e6.

Wu, P.K., Hong, S.K., Chen, W., Becker, A.E., Gundry, R.L., Lin, C.W., Shao, H., Gestwicki, J.E., and Park, J.I. (2020). Mortalin (HSPA9) facilitates BRAF-mutant tumor cell survival by suppressing ANT3-mediated mitochondrial membrane permeability. Sci. Signal. *13*, eaay1478.

Zadra, G., Ribeiro, C.F., Chetta, P., Ho, Y., Cacciatore, S., Gao, X., Syamala, S., Bango, C., Photopoulos, C., Huang, Y., et al. (2019). Inhibition of de novo lipogenesis targets androgen receptor signaling in castration-resistant prostate cancer. Proc. Natl. Acad. Sci. U S A *116*, 631–640.

STAR★METHODS

KEY RESOURCES TABLE

REAGENT or RESOURCE	SOURCE	IDENTIFIER
Antibodies		
Anti-AR, rabbit monoclonal antibody	Abcam	Cat# ab133273
Anti-Hsc/p70, rabbit monoclonal antibody	San Cruz	Cat# sc33575
Anti-Hsp27, mouse monoclonal antibody	Santa Cruz	Cat# sc59562
Anti-Hsp60, rabbit monoclonal antibody	Cell Signaling	Cat# D6F1
Anti-Hsp10, mouse monoclonal antibody	Santa Cruz	Cat# sc376313
Anti-Actin, mouse monoclonal antibody	Sigma	Cat# A5441
Chemicals, peptides, and recombinant proteins		
JG-231	Shao et al., 2018	PMID: 29953808
AUY-922	Advanced ChemBlocks Inc.	Cat # 10274
bicinchoninic acid	ThermoFisher	Cat# 23227
polybrene	Santa Cruz	Cat# sc-134220
puromycin	Gibco	Cat# A11138-03
doxycycline	Millipore-Sigma	Cat# 1226003
protease inhibitors	Sigma	Cat# P8340
Lipofectamine 2000	Thermo Fisher	Cat# 11668019
penicillin-streptomycin	Millipore-Sigma	Cat# 11074440001
oligomycin,	Selleck Chem	Cat# S1478
trifluoromethoxy carbonylcyanide phenylhydrazone (FCCP)	Cayman	Cat#15218
rotenone/antimycin A	Sigma	Cat# R8875
non heat-inactivated fetal bovine serum	Gibco	Cat# 16000044
Q5® High-Fidelity polymerase	New England BioLabs	Cat# M0492S
M-PER extraction buffer	Millipore-Sigma	Cat# GE28-9412-79
Critical commercial assays		
MN NucleoSpin® Blood Kit	Macherey-Nagel	Cat# 740951
Cyquant	Thermo-Fisher	Cat# C35011
MTT assay	Sigma	Cat# 11465007001
Deposited data		
Decipher GRID database	Karnes et al., 2018	PMID: 29760221
shRNA screening and data analysis (misc)	Kampmann et al., 2015	PMID:24992097
Experimental models: Cell lines		
Human PC-3 cell line	ATCC	CRL-1435
Human LNCaP cell line	ATCC	CRL-1740
Human C4-2 cell line	ATCC	CRL-3314
Human 22Rv1 cell line	ATCC	CRL-2505
HEK293T cell line	ATCC	CRL-3216
Oligonucleotides		
Proteostasis shRNA Library	This work	Table S1
Recombinant DNA		
dox-inducible vector, pMK1201	Kampmann et al., 2015	PMID: 26080438
packaging plasmid (pMol)	Kampmann et al., 2015	PMID:24992097
packaging plasmid (pRSV)	Kampmann et al., 2015	PMID:24992097
packaging plasmid (pVSV-g)	Kampmann et al., 2015	PMID:24992097
lentiviral backbone vector, pMK1275	Kampmann et al., 2015	PMID: 26080438

(*Continued on next page*)

Continued

REAGENT or RESOURCE	SOURCE	IDENTIFIER
Software and algorithms		
PRISM	Graphpad	https://www.graphpad.com
Wave	Agilent	https://www.agilent.com
Cluster	Eisen et al., 1998	http://bonsai.hgc.jp/~mdehoon/software/cluster/software.htm
Java TreeView	Saldanha, 2004	http://jtreeview.sourceforge.net
ImageLab	Biorad	https://www.bio-rad.com
Python	Python	https://www.python.org
Bowtie	Bowtie	http://sourceforge.net/projects/bowtie-bio/files/bowtie/1.0.0/

RESOURCE AVAILABILITY

Lead contact

Further information and requests for resources and reagents should be directed to and will be fulfilled by the Lead Contact, Jason E. Gestwicki (Jason.gestwicki@ucsf.edu).

Materials availability

Correspondence and requests for materials should be addressed to the Lead Contact.

Data and code availability

All data are available in the main text or as Supplemental information. The full list of sequences for the shRNA library are in Table S1 and the full list of p-values are in Table S2. This paper includes an analysis of existing, publically available data; for more information see (Karnes et al., 2018). All other data is available from the corresponding author upon request. This paper does not report original code. Any additional information required to reanalyze the data reported in this paper is available from the lead contact upon request

EXPERIMENTAL MODEL AND SUBJECT DETAILS

Cell lines

PC3, LNCaP, C4-2, and 22Rv1 cells were purchased from ATCC and grown in RPMI

1640 medium (Sigma R7388) supplemented with 10% non heat-inactivated fetal bovine serum (Gibco 16000044) and 1% penicillin/streptomycin (Millipore-Sigma, 11074440001). HEK293T cells (ATCC) were cultured in Dulbecco's Modified Eagle Medium (DMEM; Gibco 12430112) supplemented with 10% non heat-inactivated fetal bovine serum (Gibco 16000044) and 1% penicillin/streptomycin. All cell lines were maintained in regular tissue culture-treated flasks (Greiner C7106), with the exception of the low-adherent LNCaPs, which were kept in carboxyl-coated flasks (Corning 354778). All cells were grown at 37°C and 5% CO_2.

Lentiviral production and transduction

All lentiviruses were prepared by transfection into HEK293T cells using Lipofectamine 2000 and packaging plasmids pMol, pRSV, and pVSV-g. Viral particles were allowed to form for 48 h post transfection, and then the viral supernatant was collected, passed through a 0.45 μm filter, and stored at 4°C for no longer than one week prior to use. Viral supernatant was added to suspended cells immediately following trypsinization, along with 8 μg/mL polybrene (Santa Cruz sc-134220). The cells were allowed to adhere to the flasks, then the medium was replaced with regular growth medium after 6–8 h. After 48 h, the cells successfully infected with the lentiviral plasmids were selected with 1 μg/mL puromycin (Gibco A11138-03) for an additional 48 h. Flow cytometry was used to determine infection and selection efficiency via the expression of fluorescent markers encoded by the lentiviral vectors (generally BFP for pooled shRNA screens, and mCherry or TurboRFP for individual shRNA constructs).

METHOD DETAILS

Reagents

JG-231 was prepared in house, as described (Shao et al., 2018). AUY-922 was purchased from Advanced ChemBlocks Inc. (cat # 10274). The Proteostasis shRNA Library was prepared as previously described (Abrams et al., 2021). Briefly, sequences were cloned into the lentiviral backbone plasmid, pMK1275. For verification, individual shRNAs were cloned into either the dox-inducible backbone, pMK1201 (derived from pINDUCER10 of the Elledge Lab) or pMK1200.

Pooled shRNA screens and individual shRNA validation

Lentivirus was prepared as described above of the pooled shRNA library and used to infect the prostate cancer cell lines. Most cell lines were initially infected at ~50–60% efficiency, monitored by BFP intensity, and then were further selected with puromycin to ~100%. Immediately following the selection T0 samples, of ~4 million cells each, were collected and stored at −80°C until genomic DNA was isolated for sequencing. The cells were continually cultured, maintaining at least 4 million cells with each passage, for a period of ~10 doublings. For screens with chaperone inhibitors, the cells were dosed three times at the concentrations listed in the below Table, for a duration of 24 h each time. Concentrations were chosen by determining the IC_{50} per cell line by MTT assay, then further optimized by testing multiple concentrations at around the IC_{50} and observing the effects on cells after treatment and multiple days of recovery. Final concentrations were chosen as ones that induced cell death for a sizable population, but still allowed the cells to recover and continue growing, to reduce potential bottlenecking. At the end of the growth period, samples of ~4 million cells were collected for the Tfinal sample. For individual shRNA validation, lentivirus was prepared as described, cells were transduced and monitored by RFP intensity. Cells were then further selected with puromycin, so the final population was 50–80% RFP-positive. The percentage of RFP positive cells was then monitored by flow cytometry over a ~2 week period, with cells being split at a 1:4 ratio whenever confluency was reached.

	Screen conditions	Screen conditions
Cell line	JG-231 (μM)	AUY-922 (nM)
22Rv1	0.75	100
PC3	0.5	100
LNCaP	1	100
C4-2	1	100

Genomic DNA isolation, indexing and PCR purification

Genomic DNA was extracted using MN NucleoSpin® Blood Kit (Macherey-Nagel 740951) for ~4-6 million cells per sample. Whole genomic DNA samples were carried forward into indexing PCRs using Q5® High-Fidelity polymerase (New England BioLabs M0492S). PCR amplified, and indexed, fragments of approximately 280 bp were purified by a two-step SPRI bead purification (43), and concentrations were determined on a Qubit Fluorometer before pooling for deep sequencing on a HiSeq 4000.

Mito stress test

Stable 22Rv1 cells containing dox inducible-expressing shRNA constructs (shRNA-Hsp60-1 or Hsp60-2) were stimulated with 100 ng/mL doxycycline for 4 days prior to seeding 2.0×10^4 cells/well in a 96 well plate. Oxygen consumption (OCR) and extracellular acidification rate (ECAR) were monitored with Agilent SeaHorse XFe96 ~18h after seeding with XF DMEM pH 7.4 containing glucose, pyruvate, and glutamine. All experiments were normalized by DNA quantification with Cyquant (ThermoFisher) and are the result of at least 4 replicates per condition. Spare respiratory capacity (maximal OCR – basal OCR) and proton leakage (oligomycin-sensitive OCR – non-mitochondrial OCR) were calculated using Wave (Agilent).

Data analysis and clustering

Genes were clustered hierarchically by P-value in Cluster (Eisen et al., 1998) and displayed by Java TreeView (Saldanha, 2004).

Immunoblotting

Cells were grown in a 6-well plate to near 100% confluency, after which the medium was replaced with fresh medium containing the compounds in 1% DMSO. The compound was left on the cells and incubated at 37°C and 5% CO_2 for six hours, immediately followed by harvesting and lysing in M-PER supplemented with protease inhibitors. Lysate concentrations were quantified by a bicinchoninic acid assay (BCA, ThermoFisher 23227) and then run on 4–15% gradient SDS polyacrylamide gels at 5–10 μg of total protein per sample. All blot quantification was performed in Image Lab™ software (BioRad). The antibodies used are found in the Key Resource Table. Dilutions are as follows: Anti-AR (1:1000), Anti-Hsc70/p70 (1:200), Anti-Hsp27 (1:200), Anti-Hsp60 (1:1000), Anti-Hsp10 (1:1000), Anti-actin (1:200).

Clinical data analysis

Expression profiles of retrospective radical prostatectomy samples from 719 patients (243 with ADT treatment, 476 no treatment) were retrieved from the Decipher GRID database. Patient cohorts were pooled from two matched cohorts previously (Karnes et al., 2018). Patients were grouped based on expression of Hsp60/HSPD1. High Hsp60 was defined as higher than median expression. The additional clinical characteristics of two arms are shown in Table S3.

QUANTIFICATION AND STATISTICAL ANALYSIS

Unless otherwise specified, data plotting and statistical analyses were performed using Prism 7 (GraphPad Software). Statistical significance was evaluated by one-way ANOVA with independent post-hoc Tukey's multiple comparison test and was defined as a p-value of less than 0.05. To compare two groups, Student's t-test and two-way ANOVA were used. Details on the number of technical and biological (independent) replicates of each experiment can be found in the figure legends. In Kaplan-Meier analysis (Figure 6), the log-rank test was used to evaluate the differences in survival amongst the Hsp60 high/low groups.